Chemosphere 286 (2022) 131916

Contents lists available at ScienceDirect

Chemosphere

journal homepage: www.elsevier.com/locate/chemosphere

Review of adsorption–membrane hybrid systems for water and wastewater treatment

Sewoon Kim [a], Seong-Nam Nam [b], Am Jang [c], Min Jang [d], Chang Min Park [e], Ahjeong Son [f], Namguk Her [b], Jiyong Heo [b,*], Yeomin Yoon [a,**]

[a] Department of Civil and Environmental Engineering, University of South Carolina, Columbia, 300 Main Street, SC, 29208, USA
[b] Department of Civil and Environmental Engineering, Korea Army Academy at Yeong-Cheon, 495 Hogook-ro, Kokyungmeon, Yeong-Cheon, Gyeongbuk, 38900, South Korea
[c] School of Civil and Architecture Engineering, Sungkyunkwan University, 2066 Seobu-ro, Jangan-16 Gu, Suwon, Gyeonggi-do, 440-746, Republic of Korea
[d] Department of Environmental Engineering, Kwangwoon University, 447-1, Wolgye-Dong Nowon-Gu, Seoul, Republic of Korea
[e] Department of Environmental Engineering, Kyungpook National University, 80 Daehak-ro, Buk-gu, Daegu, 41566, Republic of Korea
[f] Department of Environmental Science and Engineering, Ewha Womans University, 52 Ewhayeodae-gil, Seodaemun-gu, Seoul, 03760, Republic of Korea

HIGHLIGHTS

- Performance of adsorption-membrane hybrid systems was reviewed for water purification.
- Adsorption-membrane hybrid systems enhanced water flux and antifouling during membrane filtration.
- Valuable information was provided for applications of adsorption-membrane hybrid systems in water industry.
- Areas of future research for adsorption-membrane hybrid systems were suggested.

ARTICLE INFO

Handling Editor: Xiangru Zhang

Keywords:
Membrane
Adsorption
Hybrid system
Water treatment
Wastewater treatment

ABSTRACT

Adsorption is an effective method for the removal of inorganic and organic contaminants and has been commonly used as a pretreatment method to improve contaminant removal and control flux during membrane filtration. Over the last two decades, many researchers have reported the use of hybrid systems comprising various adsorbents and different types of membranes, such as nanofiltration (NF), ultrafiltration (UF), and microfiltration (MF) membranes, to remove contaminants from water. However, a comprehensive evaluation of the removal mechanisms and effects of the operating conditions on the transport of contaminants through hybrid systems comprising various adsorbents and NF, UF, or MF membranes has not been performed to date. Therefore, a systematic review of contaminant removal using adsorption–membrane hybrid systems is critical, because the transport of inorganic and organic contaminants via the hybrid systems is considerably affected by the contaminant properties, water quality parameters, and adsorbent/membrane physicochemical properties. Herein, we provide a comprehensive summary of the most recent studies on adsorption–NF/UF/MF membrane systems using various adsorbents and membranes for contaminant removal from water and wastewater and highlight the future research directions to address the current knowledge gap.

1. Introduction

To meet the increasing demand for water caused by climate change, the steady population growth, and water overuse, numerous water communities have implemented water recycling systems (Kim et al., 2018). Reclaimed water is usually used for non-potable purposes, including manufacturing, agriculture, and landscaping (Shoushtarian and Negahban-Azar, 2020). The future of conventional and emerging contaminants, such as natural organic matter (NOM), heavy metals, dye chemicals, endocrine-disrupting compounds, pharmaceuticals, and personal-care products, in water resources is of great concern and the

* Corresponding author.
** Corresponding author.
E-mail addresses: jiyongheo@naver.com (J. Heo), yoony@cec.sc.edu (Y. Yoon).

https://doi.org/10.1016/j.chemosphere.2021.131916
Received 30 July 2021; Received in revised form 13 August 2021; Accepted 15 August 2021
Available online 16 August 2021

Abbreviations

BOD	Biochemical oxygen demand
COD	Chemical oxygen demand
MF	Microfiltration
MWCO	Molecular weight cutoff
NF	Nanofiltration
NOM	Natural organic matter
PAC	Powdered activated carbon
UF	Ultrafiltration
UV	Ultraviolet
WW	Wastewater

increase in contaminant consumption and water reuse are popular research topics (Al-Rifai et al., 2011). NOM plays a significant role in the most challenging issue regarding water reuse, because it is the main precursor to cancer-causing disinfection byproducts and can form complexes with heavy metals and hydrophobic compounds (Heo et al., 2012b). Toxic heavy metal cations/anions, such as Ni, As, Cr, Zn, Cu, Cd, Co, and Pb, can poison the biosphere (Carolin et al., 2017). Dangerous levels of dye chemicals from the textile, paper, and cosmetic industries have been detected in ground and surface waters (Rafatullah et al., 2010). Numerous endocrine-disrupting compounds, pharmaceuticals, and personal-care products that can pose ecological risks even at low levels (<1 μg L^{-1}) have been detected in wastewater effluents and various drinking water sources (Snyder et al., 2003; Yoon et al., 2010).

The removal of conventional and emerging contaminants in drinking water and municipal wastewater treatment plants depends on the physicochemical properties of the contaminants and treatment processes. Processes involving coagulation–flocculation–sedimentation –filtration devices (Westerhoff et al., 2005), chlorine (Huerta-Fontela et al., 2011), granular/powdered activated carbon (Jung et al., 2015), single- or multi-walled carbon nanotubes (Jung et al., 2013a), graphene oxides (Jun et al., 2019b), membranes (Yoon et al., 2002), ozone (Westerhoff et al., 2005), ultraviolet (UV) radiation (Jun et al., 2020), sonication (Im et al., 2013), and biological agents (Ryu et al., 2014) are commonly used for contaminant removal. Among treatment methods, membrane processes have been the most commonly used for water and wastewater treatment mainly owing to their high selectivity and efficiency, small footprint, low chemical use, facile scale-up/retrofication, and low sludge production (Pearce, 2007; Yoon et al., 2009; Yoon and Lueptow, 2005). In addition, adsorption is the most favorable method for various organic and inorganic contaminants for water and wastewater treatment owing to its flexibility, extensive applicability, cost-efficiency, and practicability (Chowdhury et al., 2014; Chen et al., 2019; Hong et al., 2022; Lin et al., 2019; Liu et al., 2021; Sang et al., 2021; Shi et al., 2021; Xie et al., 2021; Yuan et al., 2020).

During the last two decades, adsorption–membrane hybrid systems have been successfully used to improve membrane performance mainly by enhancing contaminant removal and reducing membrane fouling. Among different membrane processes, including forward and reverse osmosis, nanofiltration (NF), ultrafiltration (UF), and microfiltration (MF) adsorption–NF/UF/MF hybrid processes using various inorganic and organic adsorbents, such as powdered activated carbon (PAC) (Ejraei et al., 2019), zeolite nanoparticles (Esmaeili and Saremnia, 2018), graphene/graphene oxides (Gao et al., 2020; Nidamanuri et al., 2020), carbon nanotubes (Peydayesh et al., 2018), iron oxy/hydroxide agglomerates (Shemer et al., 2019), biochars (Kim et al., 2019), metal–organic frameworks (Kim et al., 2020a), and ferrocyanide/mixed cellulose esters (Xu et al., 2017), have been intensively studied. To date, hybrid processes have been effectively used for the removal of various contaminants, such as NOM (Ha et al., 2004; Heo et al., 2012a; Kang and Choo, 2010; Pearce, 2007), heavy metals (Ainscough et al., 2017; Cermikli et al., 2020; Mulyati and Syawaliah, 2018), dyes (Jirankova et al., 2007; Kim et al., 2020b; Peydayesh et al., 2018), pharmaceuticals (Alvarino et al., 2017; Sarasidis et al., 2017; Secondes et al., 2014), endocrine-disrupting compounds (Heo et al., 2012a; Kim et al., 2008), boron (Guler et al., 2011b), heavy crude oil (Cunha et al., 2019), phosphates (Ipek et al., 2012), and nitrates (Kalaruban et al., 2018).

Although many researchers have analyzed the removal of inorganic and organic contaminants using adsorption–membrane processes, the removal mechanisms and effects of the operating conditions on the transport of contaminants through various adsorbents and NF, UF, and MF membranes have not been comprehensively evaluated yet. Consequently, a systematic review of contaminant removal via adsorption–membrane treatment is critical, because the transport of inorganic and organic contaminants by hybrid membranes is considerably affected by the contaminant properties, water quality parameters, and adsorbent/membrane physicochemical properties. Therefore, herein, we comprehensively review the most recent literature on the adsorption–NF/UF/MF membrane treatments of different contaminants in water and wastewater and highlight future research direction to address the current knowledge gap. In particular, we evaluated several parameters, such as the contaminant physicochemical properties (*e.g.*, type, size, charge, and hydrophilicity), water quality parameters (*e.g.*, pH, initial concentration, temperature, ionic strength, and NOM), adsorbent properties (*e.g.*, shape, pore volume, charge, functional groups, and hydrophobicity), and membrane properties and operating conditions (*e.g.*, material, hydrophobicity, pore size, porosity, charge, operating mode, and pressure), which affect contaminant transport during adsorption–membrane filtration hybrid processes.

2. Adsorption–membrane hybrid systems

2.1. Adsorption–NF hybrid systems

2.1.1. Organic compounds

NOM: Adsorption, photocatalytic oxidation, and membrane filtration were used to achieve the optimal configuration for the treatment of pulp and paper plant wastewater (Ejraei et al., 2019). Hybrid processes using PAC or TiO_2 nanoparticles as adsorbents, UV irradiation for photocatalytic oxidation, and polymeric membranes mixed with polyacrylonitrile, polyvinylpyrrolidone, or dimethylformamide for filtration outperformed single-stage processes in terms of removal of chemical oxygen demand (COD; 88–92%), biochemical oxygen demand (BOD; 86–91%), detergents (84–91%), and total suspended solids (91–98%). In addition, previous reports indicated that adsorption and photocatalytic oxidation removed membrane foulants, caused a significant decrease in membrane flux, and a decrease in COD/BOD removal to 65%/58% and 79%/80%, respectively. In particular, the COD and BOD were either oxidized or adsorbed by TiO_2 catalysts/adsorbents under UV irradiation (Machado et al., 2007). The decrease in wastewater pH to 6.3 was attributed to the adsorption of anionic compounds on TiO_2 or their oxidation under UV irradiation and caused a decrease in the amount of detergent in the feed during photocatalytic oxidation (Adak et al., 2005).

Adsorbent–membrane systems featuring lignite-, coconut-, mineral coal-, and diverse-based adsorbents and polyethersulfone NF membranes with nominal molecular weight cutoffs (MWCO) of 1000 Da were used to remove organic substances from water samples collected from a pilot wastewater reclamation plant (Meier and Melin, 2005). Liquid chromatography–organic carbon detection was used to characterize various foulants, such as polysaccharides and large/low molecular weight acid/neutral/amphiphilic substances (Huber, 1998). During plant operation (0–1000 h) using 1000 mg L^{-1} of a lignite-based adsorbent at a 50% water recovery rate, the preliminary increases in membrane resistance and subsequent constant gradient were 3.0×10^{14} and 0.9×10^{14} m^{-1}, respectively (Meier and Melin, 2005). These findings were ascribed to the organic load (*i.e.*, polysaccharides) and

adsorbent particles clogging the membrane surface pores, because polysaccharides (MWCO >20,000 Da) and adsorbent particles (MWCO ≈ 100,000 Da) were much larger than the membrane pores. However, once the organic matter was completely removed via adsorption on PAC, the membrane flux became somewhat stable on a relatively high level. In addition, the layer of adsorbent particles on the membrane surface caused a decrease in membrane rejection for inorganics owing to concentration polarization in the particle layer.

Endocrine-disrupting compounds: Electrostatically immobilized iron (III) tetrasulfophthalocyanine on Amberlite IRA-400 anion-exchange resin was used as the adsorbent/catalyst in an adsorption–NF hybrid system utilized to remove bisphenol A, which is a strong endocrine disruptor (Kim et al., 2008). Preliminary bisphenol A removal experiments were performed using pure Amberlite IRA-400, Amberlite IRA-400 in the presence of H_2O_2, iron(III) tetrasulfophthalocyanine + Amberlite IRA-400, and iron(III)-tetrasulfophthalocyanine + Amberlite IRA-400 in the presence of H_2O_2 to evaluate the role of Amberlite IRA-400 during bisphenol A removal in the absence and presence of iron (III) tetrasulfophthalocyanine in the exchange column. A significant amount (~70%) of bisphenol A was removed after 2 h of contact using pure Amberlite IRA-400. Owing to its abundant pores, Amberlite IRA-400 is hydrophobic; therefore bisphenol A removal using Amberlite IRA-400 occurred mainly via adsorption. The bisphenol A removal efficiencies during the first three experiments were not significantly different, indicating that H_2O_2 alone could not oxidize bisphenol A directly, and iron(III) tetrasulfophthalocyanine did not improve the adsorption ability of Amberlite IRA-400. However, Amberlite IRA-400 + iron(III) tetrasulfophthalocyanine in the presence of H_2O_2 oxidized bisphenol A. During bisphenol A removal via NF, the residual concentration of bisphenol A increased quickly with time, because more than 85% of bisphenol A was removed via NF and concentrated in the reactor (Kim et al., 2008). Nevertheless, the increase in bisphenol A concentration in the reactor of the adsorption–NF hybrid system was considerably lower than that in the reactor of the NF membrane system. This change was ascribed to bisphenol A adsorption by Amberlite IRA-400. Moreover, the addition of H_2O_2 to the bisphenol A reactor after 15 h did not cause the bisphenol A concentration to increase further, presumably because the presence of H_2O_2 prompted the catalytic degradation of bisphenol A.

Levofloxacin, a synthetic antibiotic used to treat various bacterial infections, is mainly excreted through human/animal urine and feces (Schlusener and Bester, 2006). A magnetic carbon nanocomposite fabricated from pineapple waste biomass as a precursor was used to remove levofloxacin in an adsorption–NF hybrid system featuring a NF membrane with a salt rejection of 97% (Ullah et al., 2019). Levofloxacin was adsorbed relatively quickly onto the nanocomposite during the early stages of a 280-min kinetic study, and equilibrium was reached within 1 h. The rapid initial adsorption of levofloxacin was attributed to the abundance of accessible sites on the prepared adsorbent (surface area = 39 $m^2\ g^{-1}$; total pore volume = 0.2 $cm^3\ g^{-1}$; average pore diameter = 1.975 nm). In the pH range of 3–7, levofloxacin adsorption increased with increasing pH owing to cationic interchange (Thunemann et al., 2006). However, at pH > 7, the amount of levofloxacin$^+$ decreased slowly and levofloxacin molecules were converted to levofloxacin $^{\pm}$ zwitterions. At alkaline pH levofloxacin molecules in solution were converted into levofloxacin$^-$ and the amount of levofloxacin adsorbed decreased significantly. The retention of the magnetic carbon nanocomposite–NF membrane hybrid system was very high (~100%) and its permeate fluxes were also high (Ullah et al., 2019). After the 1-h test cycle, the membranes were washed with deionized water. The total backwashing time of the membranes and magnetic carbon nanocomposite was considerably shorter than that of the pristine membranes, because the magnetic carbon nanocomposite was completely removed from the slurry using a magnet (Tanis et al., 2008).

Dye chemicals: Positively charged hybrid NF membranes, which were fabricated via a phase inversion method by embedding triethylenetetramine-functionalized multi-walled carbon nanotubes into a polyethersulfone support, were used for the removal of several dyes, including rhodamine B, crystal violet, orange G, and indigo carmine (Peydayesh et al., 2018). Increasing the loading of triethylenetetramine-functionalized multi-walled carbon nanotubes from 0.4 to 0.8 wt% led to an increase in membrane pore size from 0.73 to 0.86 nm, respectively. These pores were wider than those of the pristine polyethersulfone membrane (0.65 nm) owing to the immediate demixing that occurred during phase inversion. To evaluate the effect of membrane surface charge on dye removal, the flux and removal of the hybrid membranes for four electrolytes were determined. Electrolyte removal using the hybrid NF membranes decreased as follows: $MgCl_2$ > $MgSO_4$ > Na_2SO_4 > NaCl, whereas electrolyte removal using pristine polyethersulfone NF membranes decreased as follows: Na_2SO_4 > $MgSO_4$ > $MgCl_2$ > NaCl. These findings suggested that ion size and the electrostatic interactions between the membrane surface and the electrolytes in solution affected membrane performance (Tang et al., 2015). Similar membranes fluxes were observed for the aforementioned dye chemicals; however, their removal rates varied depending on the compound, as follows: cationic dyes (99.2% and 98.4% for rhodamine B and crystal violet, respectively) > anionic dyes (87.1% and 82.1% for indigo carmine and orange G, respectively), confirming the significant role of Donnan exclusion for membrane performance. In addition, dye removal was affected by particle size and depended on the molecular weight of the dye: rhodamine B (479 g mol^{-1}) > indigo carmine (466 g mol^{-1}) > orange G (452 g mol^{-1}) > crystal violet (408 g mol^{-1}) (Zhong et al., 2012). Membrane flux decreased with increasing rhodamine B concentration in the range of 50–200 mg L^{-1} owing to increasing osmotic pressure with concentration; moreover, rhodamine B removal decreased with increasing concentration because the electrostatic interactions between the dye and membrane weakened and became negligible with increasing dye concentration (Zhao et al., 2016). The fouling of the hybrid membrane with a triethylenetetramine/multi-walled carbon nanotube loading of 0.4% decreased rapidly and irreversibly to 6.9%, whereas the fouling of the pristine membrane decreased to 27%. In addition, these findings indicated that the hybrid membranes could be reused for many cycles because they retained their high efficiency after simple hydraulic cleaning (Peydayesh et al., 2018).

Other contaminants: The presence of total petroleum hydrocarbons (mixtures of hydrocarbons in crude oil) in the environment is a major global issue (Aguilar-Arteaga et al., 2010). Recently, numerous materials and advantageous methods for separating total petroleum hydrocarbons from oil-polluted wastewater have been studied (Esmaeili and Sadeghi, 2014). Surfactant (hexadecyltrimethylammonium bromide)-modified granulated NaA zeolite nanoparticles were used as the adsorbent in combination with polyaniline NF membranes to separate total petroleum hydrocarbons from the wastewater generated by an oil refinery (Esmaeili and Saremnia, 2018). In this hybrid system, the adsorption column (height = 20 cm) containing NaA zeolite nanoparticles and nanofiltration tubes was used continuously at a filtration rate of 26.3 mL min^{-1}. This hybrid system exhibited an outstanding removal efficiency of 99.8% for total petroleum hydrocarbons. The highest removal efficiency of the pure adsorbent in the dosage range of 2.5–12.5 mg L^{-1} was 92.3%. The adsorption capacity of the pure adsorbent was analyzed in the pH range of 3–11, and the highest adsorption capacity was achieved at pH 7. The adsorbent surface became negatively charged in the presence of H_3O^+ ions, hindering the adsorption process. Small H_3O^+ ions could travel quickly through the zeolite pores and replace the exchangeable ions of the adsorbent (Kong et al., 2006). Therefore, the removal efficiency of the adsorbent decreased with increasing H_3O^+ concentration. Similar findings were reported by Torabian et al. (2010). As the operating pressure increased from 3 to 9 bar, the membrane flux and removal rate of total petroleum hydrocarbons increased from 33.3 to 69.7 kg $m^{-2}\ h^{-1}$ and 89.0%–99.7%, respectively. Moreover, the average size of the membrane pores increases with increasing pressure owing to the increase in liquid

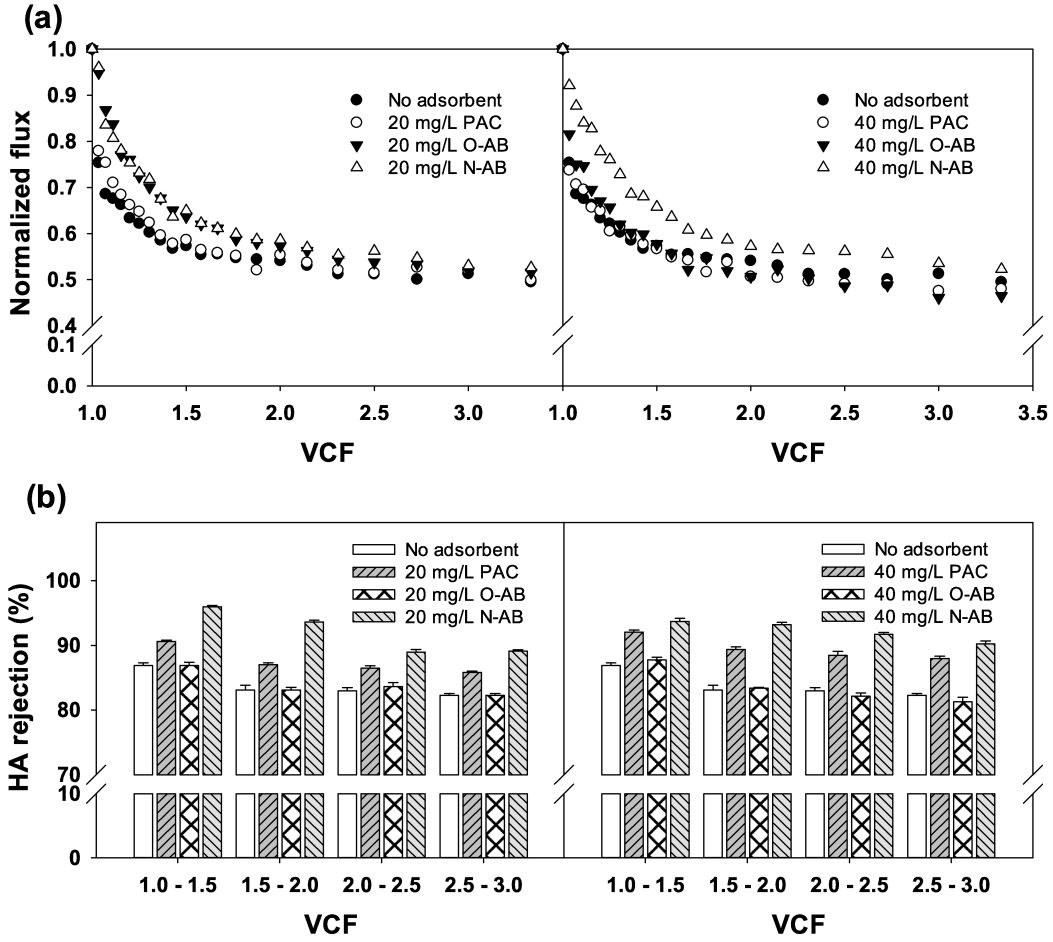

Fig. 1. Influence of adsorbent concentration on flux decline and (humic acid) HA rejection: (a) Flux decline with 20 mg L^{-1} (left) and 40 mg L^{-1} (right) adsorbents, and (b) HA rejection with 20 mg L^{-1} (left) and 40 mg L^{-1} (right) adsorbents; O-/N-AB = oxygen/nitrogen-based activated biocar; VCF = volume concentration factor. Operating conditions: ΔP = 350 kPa (50 psi); pH = 7; conductivity = 300 μS cm^{-1}; initial HA concentration (before pretreatment via adsorption) = 5 mg L^{-1} as dissolved organic carbon for a 2 h contact time (Chu et al., 2017).

pressure and density ascribed to the cross-sectional flow (Esmaeili and Saremnia, 2018).

2.2. Adsorption–UF hybrid systems

2.2.1. Organic compounds

NOM: Chlorination pretreatment is frequently used in drinking water treatment plants for disinfecting and controlling the taste/odor-causing compounds, which can affect the removal of inorganic/organic compounds via adsorption and/or membrane filtration (Wang et al., 2016). Therefore, the effect of chlorination pretreatment on NOM removal from surface (river) water was analyzed using an adsorption–UF hybrid system with iron oxide particles as the adsorbent (Ha et al., 2004). Prechlorination changed the properties of the dissolved NOM and colloidal matter in the feed water, resulting in lower NOM removal using the hybrid system. The presence of iron oxide particles in suspension or a cake layer increased NOM retention in the hybrid system, presumably owing to adsorption or a steric exclusion effect. The added iron oxide particles significantly improved the membrane flux, because they removed NOM, which can cause membrane fouling (Yoon et al., 2005). The membrane flux in prechlorinated feed water was relatively low for both the hybrid and UF systems, whereas the membrane permeate flux was unaffected by chlorination once colloidal matter was removed before UF. In addition, while prechlorination caused the properties of dissolved NOM to change, it did not affect membrane permeability significantly. Overall, prechlorination played an important role in decreasing the size of colloidal matter in feed water, which can subsequently reduce membrane permeate flux (Ha et al., 2004).

Recently, activated biochar prepared via partial combustion of biomass in waste or byproducts has attracted increasing attention for soil remediation, CO_2 sequestration, water purification, and wastewater treatment (Lehmann, 2007; Nguyen et al., 2007). Coal-based commercially available PAC and inexpensive oxygen- and nitrogen-based activated biochars with high inner pore site density were used as adsorbents in adsorbent–UF membrane hybrid systems to remove humic acid from soil (Chu et al., 2017). The adsorption capacity of the nitrogen-based activated biochar adsorbent for humic acid (1.31 (mg g^{-1})(mg $L^{-1})^{1/n}$) was higher than those of PAC (1.21 (mg g^{-1})(mg $L^{-1})^{1/n}$) and the oxygen-based activated biochar adsorbent (1.23 (mg g^{-1})(mg $L^{-1})^{1/n}$). The membrane flux and humic acid retention of the adsorption–UF hybrid systems decreased in the absence/presence of the adsorbents under the following experimental conditions: adsorbent dosages of 20 and 40 mg L^{-1}, pH 7, and conductivity of 300 μS cm^{-1} with NaCl (Fig. 1). The humic acid retention of the hybrid systems with PAC, oxygen-based activated biochar, and nitrogen-based activated biochar adsorbent doses of 20 mg L^{-1} was approximately 2.4%, 12%, and 13% higher, respectively, than that of the UF system in the absence of adsorbents (Fig. 1a). The water fluxes of the UF membrane paired with the oxygen-/nitrogen-based activated biochars (~22%) were considerably lower than that of the UF membrane paired with PAC (31%). These findings could be explained as follows: (i) foulant was adsorbed on each adsorbent and (ii) weak hydrophobic attractions

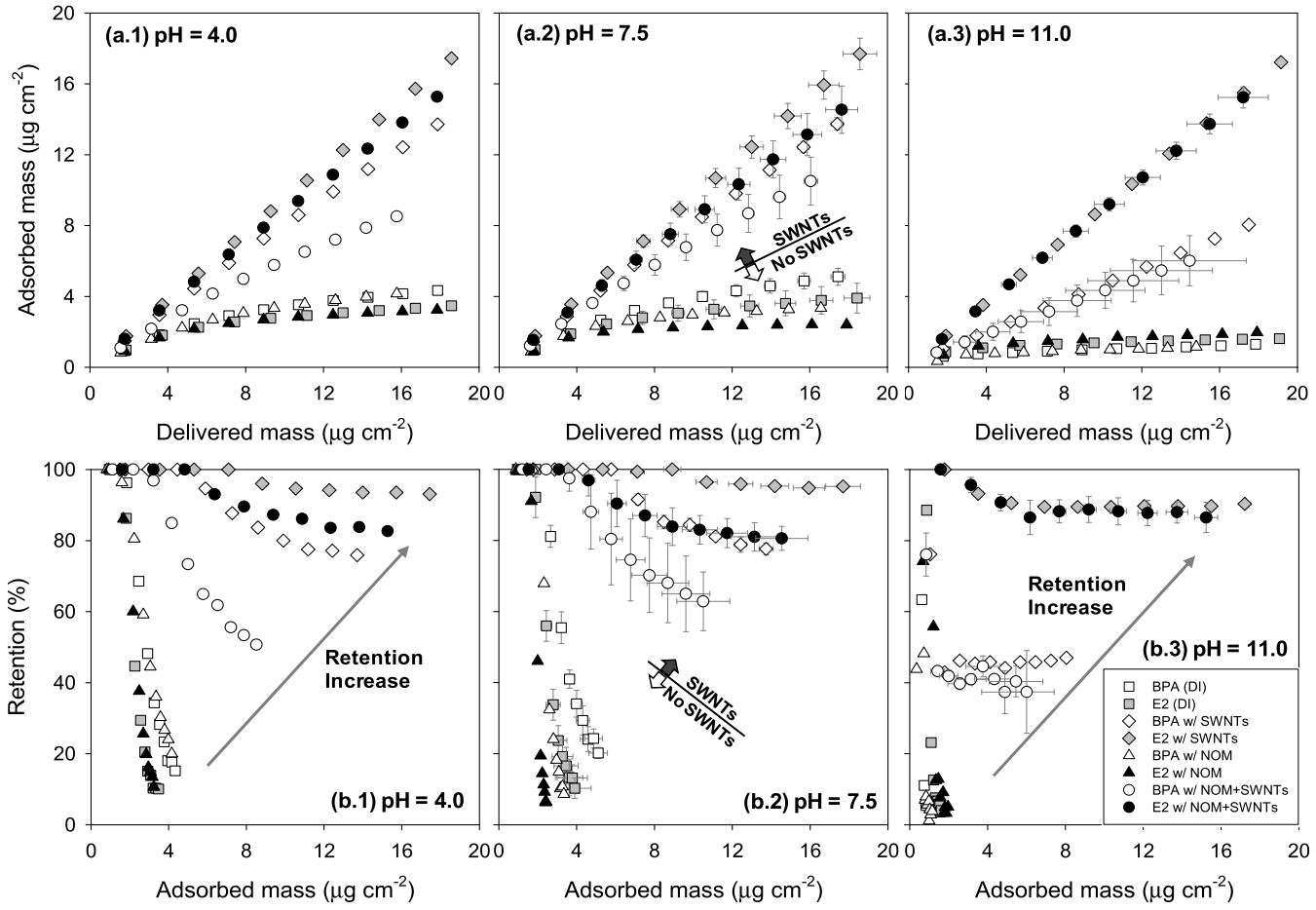

Fig. 2. Comparison of (a) delivered and adsorbed mass accumulated and (b) adsorbed mass and retention for bisphenol A (BPA) and 17α-estradiol (E2) in the UF5K filtration in the absence and presence of NOM and single-walled carbon nanotubes (SWNTs). Operating conditions: $\Delta P = 827$ kPa (120 psi); stirring speed = 300 rpm; recovery = 50%; dissolved organic carbon (NOM = humic acid) = 8 mg L^{-1}; SWNTs = 10 mg L^{-1}; conductivity = 500 μS cm^{-1}; pre-contact time with SWNTs = 2 h (Heo et al., 2012a).

occurred between the relatively hydrophilic oxygen-/nitrogen-based activated biochars and the UF membranes. The humic acid retention of the hybrid systems depended on the adsorbent and was 84%, 90%, and 92% for the systems featuring oxygen-based activated biochar, PAC, and nitrogen-based activated biochar, respectively, as the adsorbents (Fig. 1b). Particularly, the highest humic acid removal of the nitrogen-based activated biochar–UF system was attributed to the strong electrostatic interactions between the high-polar functional groups of biochar and negatively charged UF membrane (Chu et al., 2017).

Ferrihydrite, which is a mineral oxide adsorbent, and PAC were used to control NOM fouling in adsorbent–UF membrane systems (Kang and Choo, 2010). Similar NOM removal degrees were observed for the systems featuring both adsorbents; however, the decrease in fouling depended on the membrane pore size. Membranes with relatively small pores exhibited low fouling, and the relative effects of reversible and irreversible fouling resistances appeared to be minimal for such membranes. However, a relatively high degree of reversible fouling resistance was observed owing to the presence of large-size NOM molecules on the surface of membranes with large pores. These findings suggested that ferrihydrite particles can successfully control large NOM molecules and improved the flux of the adsorbent–UF membrane systems. Kim et al. used heated aluminum oxide particles as adsorbents in adsorbent–UF membrane hybrid systems, which were utilized to pretreat water prior to desalination via reverse osmosis (Kim et al., 2010). The heated aluminum oxide particles decreased membrane fouling, and the decrease in membrane fouling was directly proportional to the thickness of the layer of heated aluminum oxide particles. Because fouling was negligible, the membrane could be used continuously without cleaning for extended periods (up to a few days). Shao et al. examined the combined fouling effects of humic acid and PAC in the absence and presence of 0.5 mM Ca^{2+} ions on membrane fouling, humic acid removal, and PAC deposition (Shao et al., 2016). In the absence of Ca^{2+} ions, humic acid removal increased with the addition of PAC owing to the hindered foulant back diffusion effect associated with Brownian and shear-induced diffusion (Shi et al., 2011). In addition, humic acid removal increased with increasing PAC particle size. However, in the presence of Ca^{2+} ions, membrane fouling occurred mainly via steric effects (Shao et al., 2016).

Endocrine-disrupting compounds and pharmaceuticals: Single- and multi-walled carbon nanotubes with hexagonal carbon lattice structure have drawn increasing attention owing to their exceptional properties and numerous potential environmental applications (Mauter and Elimelech, 2008; Pan and Xing, 2008). The removal and adsorption of bisphenol A and 17β-estradiol, which are well-known endocrine-disrupting compounds, were studied using single-walled carbon nanotube–UF membrane hybrid systems in a dead-end stirred cell setup (Heo et al., 2012a). Batch adsorption and membrane filtration tests indicated that adsorption can be used to remove significant amounts of these hydrophobic compounds. The adsorption rates of bisphenol A and 17β-estradiol varied from ~7% to 95%, depending on the solution pH and presence of humic acid and single-walled carbon nanotubes (Fig. 2). The presence of humic acid led to a significant decrease in the

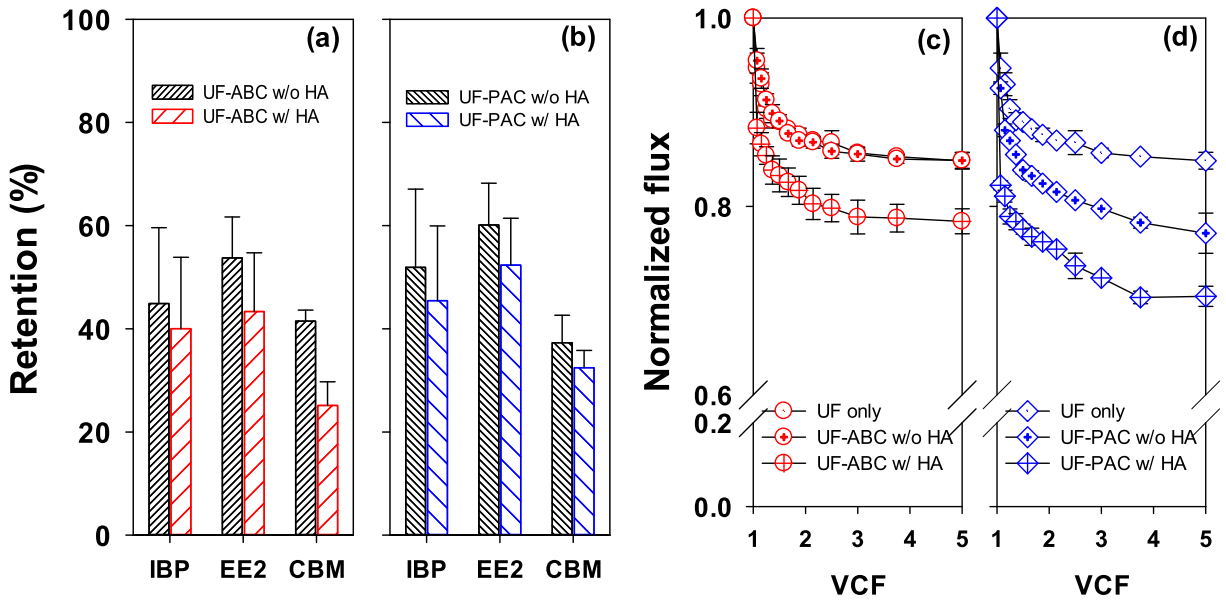

Fig. 3. Ibuprofen (IBP), 17 α-ethinyl estradiol (EE2), and carbamazepine (CBM) retention by (a) UF-activated biochar (ABC) and (b) UF-PAC. Comparison of normalized flux decline: (c) UF only, UF-ABC without humic acid (HA), and UF-ABC with HA, and (d) UF only, UF-PAC without HA, and UF-PAC with HA. Operation conditions: ΔP = 520 kPa (75 psi); stirring speed = 300 rpm; pH = 7; conductivity = 300 μS cm^{-1}; HA = 5 mg L^{-1}as dissolved organic carbon; ABC = 10 mg L^{-1}; PAC = 10 mg L^{-1}; pre-contact time with ABC and PAC = 4 h (Kim et al., 2019).

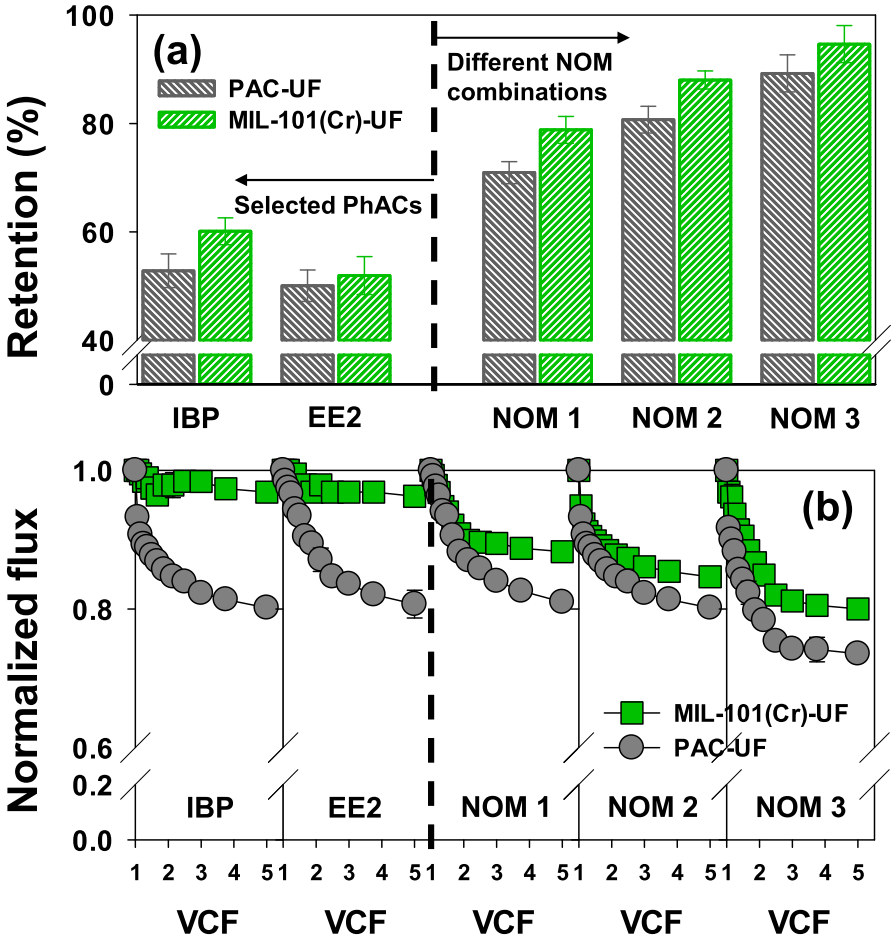

Fig. 4. (a) Retention rate and (b) normalized flux decline of selected pharmaceuticals and different NOM combinations by MIL-101(Cr)-UF and PAC-UF. Operation conditions: ΔP = 520 kPa; stirring speed = 200 rpm; metal-organic framework (MOF) = 20 mg L^{-1}; initial selected pharmaceuticals concentration = 10 μM; initial NOM = 10 mg L^{-1}as dissolved organic carbon; pH = 7.0; conductivity = 300 μS cm^{-1}; pre-contact time with MOF = 2 h (Kim et al., 2020a).

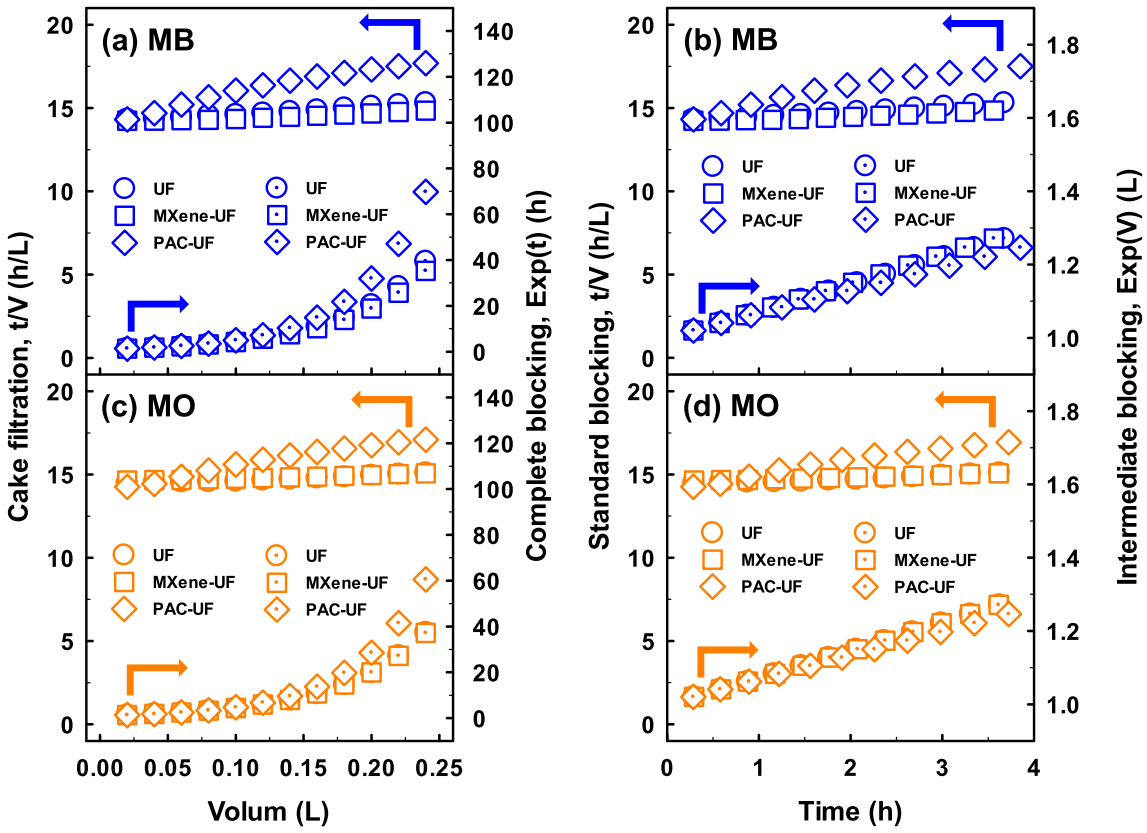

Fig. 5. Four conceptual blocking law models at 75 psi (520 kPa) in the single UF, MXene-UF and PAC-UF system. (a) Cake filtration and complete blocking analysis for methylene blue (MB, (b) standard blocking and intermediate blocking analysis for MB, (c) cake filtration and complete blocking analysis for methyl orange (MO), and (d) standard blocking and intermediate blocking analysis for MO (Kim et al., 2020b). (For interpretation of the references to colour in this figure legend, the reader is referred to the Web version of this article.)

adsorption capacity of the hybrid system for bisphenol A and 17β-estradiol, while compound retention via adsorption was significant in the presence of single-walled carbon nanotubes and single-walled carbon nanotube–humic acid combinations. The removal and adsorption trends of the target contaminants using single-walled carbon nanotube—UF membrane hybrid systems were considerably affected by the interactions between bisphenol A or 17β-estradiol and humic acid, single-walled carbon nanotubes, and the UF membrane. Previous studies have demonstrated that a decrease in compound adsorption was anticipated in the presence of different types of NOM owing to the interactions between NOM and the endocrine-disrupting compounds and their direct competition for the available adsorption sites of the single-walled carbon nanotubes (Chen et al., 2008; Zhang et al., 2010). The amounts of retained and adsorbed bisphenol A and 17β-estradiol at pH 4 and 7.5 were similar and decreased significantly at pH 11 (Heo et al., 2012a). This was attributed to the difference in compound hydrophobicity, which was assessed using the octanol–water partition coefficients of the contaminants at different pH levels. At pH > ~10.5, the bisphenol A and 17β-estradiol molecules become anionic; therefore, adsorption decreased owing to the electrostatic repulsions between the negatively charged bisphenol A or 17β-estradiol, negatively charged membrane, and single-walled carbon nanotubes (Pan and Xing, 2008).

The removal of ibuprofen, 17 α-ethinyl estradiol, and carbamazepine pharmaceuticals was evaluated using UF membranes combined with activated biochar with excellent aromatization and porous properties (Kim et al., 2019). The average removal rates for ibuprofen, 17 α-ethinyl estradiol, and carbamazepine by the UF, activated biochar–UF membrane system, and activated biochar–UF membrane system in the presence of humic acid at pH 3.5, 7, and 10.5 were 24%, 15%, and 7%; 42%, 53%, and 41%; and 37%, 43%, and 24%, respectively. The average pharmaceutical removal rates of the UF membrane decreased as follows: ibuprofen >17 α-ethinyl estradiol > carbamazepine; however, the average removal rate of the activated biochar–UF system for 17 α-ethinyl estradiol was higher than those of ibuprofen and carbamazepine. To assess the efficiency of the activated biochar–UF membrane systems, their removal rates and water flux performances at pH 7 were compared with those of a commercial PAC–UF membrane system (Fig. 3). The findings suggested that removal rates of the PAC–UF membrane system were approximately 4–7% and 6–9% higher in the absence and presence of humic acid, respectively, than those of the activated biochar–UF membrane systems. The high aromaticity of activated biochar enhanced adsorption (Jung et al., 2013c; Nguyen et al., 2007); however, the small surface area and pore volume of activated biochar limited its adsorption ability (Ji et al., 2010; Nguyen et al., 2007). The normalized flux of the PAC–UF membrane system in the absence of humic acid was 0.76 and decreased rapidly to ~0.70 in the presence of humic acid. This was ascribed to fouling caused by pharmaceuticals, PAC, and/or humic acid, which clogged the membrane surface and pores, causing a decrease in flux. PAC can remove pharmaceuticals via adsorption; however, it can also be easily deposited on membrane surfaces owing to its high adsorption capability. Therefore, the water flux of the PAC–UF membrane system was significantly lower than that of the UF membrane. The pharmaceutical removal capacity of the PAC–UF membrane system was higher than that of the activated biochar–UF membrane system because PAC was more hydrophobic than activated biochar. Moreover, the surface area and pore volume of PAC were higher than those of activated biochar, and the membrane flux of the activated biochar–UF membrane system was higher than that of the PAC–UF membrane system (Kim et al., 2019).

Metal–organic frameworks are versatile compounds that can be used

for catalysis (Ma et al., 2010), separation processes (Rodenas et al., 2015), and gas storage (Yoo et al., 2020), owing to their unique properties, including tenability, large surface area, high porosity, and abundant coordinatively unsaturated sites. A MIL101(Cr) metal–organic framework–UF membrane hybrid system was used to remove pharmaceuticals (ibuprofen and 17α-ethinyl estradiol) and NOM (humic/tannic acid) (Kim et al., 2020a). The removal capacity and membrane flux of the MIL101(Cr)–UF membrane hybrid system were compared with those of a commercial PAC–UF membrane hybrid system (Fig. 4). The removal capacities of the MIL101(Cr)–UF membrane hybrid system for ibuprofen, 17α-ethinyl estradiol, and NOM (which comprised NOM1, NOM2, and NOM3 with humic-to-tannic acid ratios of 10:0, 5:5, and 0:10, respectively) were 7%, 2%, and 5–8% higher, respectively, than those of the commercial PAC–UF membrane hybrid system. Furthermore, the removal capacity of the MIL101(Cr)–UF membrane hybrid system for NOM depended on the humic-to-tannic acid ratio. The higher removal capacities of the MIL101(Cr)–UF membrane hybrid system were ascribed to the differences in textural properties between MIL-101 (Cr) and PAC. Even though the pore diameters of the adsorbents were comparable (2.5 and 2.2 nm for MIL-101(Cr) and PAC, respectively), the adsorption ability of MIL-101(Cr) was ascribed to its total pore volume (1.4 $cm^3\ g^{-1}$) being higher than that of PAC (0.24 $cm^3\ g^{-1}$). The normalized fluxes of the MIL101(Cr)–UF membrane hybrid system for ibuprofen, 17α-ethinyl estradiol, NOM1, NOM2, and NOM3 at a volume concentration factor of 5 were 0.97, 0.96, 0.88, 0.85, and 0.80, respectively, which were higher than those of the commercial PAC–UF membrane hybrid system (0.83, 0.81, 0.81, 0.80, and 0.74, respectively). MIL-101(Cr) produced somewhat negligible fouling in the presence of the pharmaceuticals; however, PAC, which was more hydrophobic than MIL-101(Cr), can deposit on the polyamide membrane surface and cause noticeable fouling (Perreault et al., 2014). Therefore, the fluxes of the PAC–UF membrane hybrid system for ibuprofen and 17α-ethinyl estradiol were significantly lower than those of the MIL-101 (Cr)–UF membrane hybrid system. Even though the normalized flux performance of the MIL-101(Cr)–UF membrane hybrid system was higher than that of the PAC–UF membrane hybrid system, the normalized fluxes of both systems decreased significantly (Fig. 4).

Dye chemicals: MXenes are a novel class of multilayered two-dimensional inorganic nanomaterials with numerous applications, including energy storage/delivery devices, transparent conductive electrodes, and water treatment systems (Jun et al., 2019a). A MXene–UF membrane hybrid system comprising titanium carbide ($Ti_3C_2T_x$) MXene and a polyamide thin film composite membrane (MWCO = 3000 Da) was used to remove methylene blue and methyl orange dyes (Kim et al., 2020b). To evaluate the decrease in flux of the system for methylene blue and methyl orange in detail, permeate flux modeling was performed for the UF membrane and the MXene–UF and PAC–UF membrane hybrid systems. Because the cake layer of the MXene–UF membrane system was thinner than that of the UF membrane, the membrane filtration index rate of the MXene–UF membrane system was smaller than that of the UF membrane. This indicated that the MXene increased membrane flux owing to the electrostatic repulsions between MXene and the membrane. However, it appeared that PAC acted as a foulant because the membrane flux of the PAC–UF membrane hybrid system was lower than that of the UF membrane owing to PAC deposition on the membrane surface. Moreover, the membrane filtration index rate of the PAC–UF membrane hybrid system was higher than that of the UF membrane, further confirming that PAC acted as foulant, because membrane filtration index rate increases with increasing cake formation. Four conceptual blocking models (cake filtration and complete, standard, and intermediate blocking), which have been commonly used to assess membrane fouling (Chu et al., 2016), were evaluated to explain the fouling mechanism (Fig. 5). For the UF membrane, the fitting coefficients of the cake filtration model ($r^2 = 0.996$ for methylene blue and 0.958 for methyl orange) were somewhat greater than those of the standard blocking model ($r^2 = 0.995$ for methylene blue and 0.952 for methyl orange); however, the fitting coefficients of the aforementioned models were higher than those of the complete ($r^2 = 0.901$ for methylene blue and 0.904 for methyl orange) and intermediate blocking ($r^2 = 0.901$ for methylene blue and 0.902 for methyl orange) models. These findings were attributed to cake filtration caused by dye buildup in the cake layer. Furthermore, because the size of methylene blue and methyl orange molecules (~2.0 nm) was considerably smaller than the diameter of the membrane pores (2.6–3.0 nm), a fraction of each dye could be adsorbed into the membrane pores via hydrogen-bonding (Ma et al., 2012). The fitting coefficient of the cake filtration model for the removal of methylene blue using the MXene–UF membrane hybrid system was higher than those of the complete, standard, and intermediate blocking models, whereas the fitting coefficients of the cake filtration and standard blocking models for the removal of methyl orange using the MXene–UF membrane hybrid system were higher than those of the complete and intermediate blocking models. These results suggested that methylene blue could be adsorbed on the $Ti_3C_2T_x$ MXene via electrostatic attraction, which decreased internal membrane fouling (Zheng et al., 2018). The fitting coefficients of the cake filtration model for the removal of both dyes using the PAC–UF membrane hybrid system were the highest of all models, presumably owing to the deposition of large PAC amounts on the membrane surface (Kim et al., 2020b). A previous study compared the mechanical strength of the MXene-based composite membrane versus the print paper substrate for efficient oil/water separation, which verifies that the MXene membrane holds superior mechanical strength and ductility owing to its greater breakage pressure and deflection (Saththasivam et al., 2019). The breakage pressure increased from 107 to 165 kPa once the print paper was coated with delaminated MXene, which shows an increase of approximately 55%.

An adsorption–membrane hybrid system comprising MCM-41, which is a mesoporous material, and polyvinyl chloride hollow fiber with an overall pore size of 0.01–0.1 μm as the adsorbent and UF membrane material, respectively, was used to remove Lanasyn S, a dye chemical, from synthetic and real textile and leather industry wastewater (Alardhi et al., 2020). Experiments were performed using actual wastewater samples containing 10 mg L^{-1} Lanasyn S at full retentate recycle. The experimental conditions were as follows: adsorbent mass = 20 mg, pH 6, temperature = 25 °C, pressure = 100 kPa, and flow rate = 100 mL min^{-1}. The permeate flux in the hybrid system was stable, because membrane fouling was controlled during the experiments (Kim et al., 2009). The mesoporous material removal of the membrane via filtration caused the deposition of a porous layer on the membrane surface. This layer acted as an active secondary layer to retain the inorganic and/or organic compounds in wastewater that cannot be removed via adsorption (Tomaszewska and Mozia, 2002). The maximum permeate fluxes achieved for synthetic and actual wastewater samples were 41 and 39 L $m^{-2}\ h^{-1}$, respectively, and the maximum removal rates were 97.7% and 94.8%, respectively (Alardhi et al., 2020).

Other contaminants: Phenol and its derivatives are present the industrial wastewater from the paper, ceramic, conversion, and dye industries and are known human carcinogens. Moreover, exposure to small amounts of phenol and its derivatives can cause mental disorders (Srihari and Das, 2008). The effectiveness of hypercrosslinked polymer adsorbent–UF membrane (pore size = 0.04 μm) hybrid systems for phenol removal from synthetic wastewater samples was analyzed (Ipek et al., 2012). Phenol removal increased upon increasing the adsorbent dose of the hybrid system from 1000 to 4000 mg L^{-1}. The phenol removal of the hybrid system increased from 65% to 80%, 89%, and 92% with the increase in adsorbent dose from 1,000, to 2,000, 3,000, and 4000 mg L^{-1}, respectively. Guler et al. reported similar results for the removal of boron; the concentration of boron in the membrane permeate decreased with increasing adsorbent resin dose of the hybrid system (Guler et al., 2011a). The optimal operational flow rate for phenol removal from permeates using fresh and saturated adsorbent samples was approximately 6 mL min^{-1} and the lowest phenol concentration was achieved using an adsorbent dose of 3000 mg L^{-1}. Once

the replacement amount was increased steadily, phenol adsorption increased owing to the synchronization of the improvement of chance for the new adsorbent to interact with the phenol in the solution and removal of used adsorbent (Ipek et al., 2012).

Accidental crude oil spills in water environments are more concerning than spills on soil, because wind or waves can spread the oil film formed at the water surface, significantly expanding the contaminated region (Matin et al., 2018). The effectiveness of hybrid systems comprising magnetic inorganic–organic hybrid materials as adsorbents and a polyethersulfone UF membrane for removing crude oil from water surfaces was evaluated (Cunha et al., 2019). Coconut mesocarp, sugarcane bagasse, sawdust, and water hyacinth were used as biomass waste-based adsorbents, and the sugarcane-bagasse-based adsorbent presented the highest oil removal efficiency (~85%, adsorption capacity = 17,000 mg g^{-1}), which was ascribed to the fibrous properties of the material. The sugarcane bagasse–UF membrane system removed 35 times its own mass in oil (adsorption capacity = 35,000 mg g^{-1}). In addition to its remarkable removal efficiency, the sugarcane bagasse–UF membrane system allowed the mechanical elimination of oil from the membrane surface. This is advantageous because it eliminates the need for subsequent slow abstraction stages, which require large volumes of organic solvents and amounts of energy (Cunha et al., 2019).

2.2.2. Inorganic compounds

Cationic heavy metal contaminants: The presence of heavy metals in water and wastewater is a significant public health concern, because most heavy metals, such as cadmium and lead, are nonbiodegradable (Senguttuvan et al., 2021). An adsorbent–UF membrane hybrid system featuring Aceh natural zeolite as the adsorbent (adsorbent dosage = 10–100 mg L^{-1}) and a polyethersulfone (MWCO = 20,000 Da) UF membrane was used to remove cadmium and lead (Mulyati and Syawaliah, 2018). Adsorption occurred rapidly during the first 20 min, then the amounts of adsorbed metal increased gradually, and adsorption reached equilibrium after 80 min. These results were attributed to the decrease in the number of active sites or contact surface area of the adsorbent. Additionally, adsorption capacity depends on the number of metal molecules that travel from the bulk liquid phase to the active sites of the adsorbent (Jiang et al., 2010). Solution pH can affect the adsorbent surface charge and the chemical equilibrium between adsorbate and adsorbent (Aloma et al., 2012). In the solution pH range of 2–9, the adsorption of cadmium and lead increased rapidly with increasing pH owing to decreasing competition between the target metal ions and H_3O^+ ions, and then reached a maximum at pH 7. The highest removals of cadmium and lead via zeolite adsorption were 86% and 89%, respectively, and the treated water samples did not meet drinking water quality standards (5 and 10 μg L^{-1} for cadmium and lead, respectively). In addition, the permeate concentrations of cadmium and lead during membrane removal were 210 and 242 μg L^{-1}, respectively. Therefore, the adsorption and UF membrane removal processes could be combined into a hybrid system to decrease the cadmium and lead content in water (Mulyati and Syawaliah, 2018).

Anionic heavy metal contaminants: The World Health Organization regulated the levels of the essential element boron in drinking and irrigation water to 2.4 and 1 mg L^{-1}, respectively (Rerkasem et al., 2020). Considering the toxicity of arsenic and its high content in geothermal water, the United States Environmental Protection Agency has set the arsenic standard for drinking water to 10 μg L^{-1} (Nigra and Navas-Acien, 2020). A novel N-methyl-D-glucamine-functionalized revealing gel, an expanded gel, and an epidermal-like structure were used as adsorbents for the instantaneous removal of boron and arsenic from saline geothermal water utilizing adsorption–hollow-fiber UF membrane hybrid systems (Cermikli et al., 2020). The effects of the adsorbent concentration and resin replacement rate (6–12 mL min^{-1}) for boron removal from geothermal water were analyzed. Boron removal using the hybrid system with the gel-based resin adsorbent increased from 66% to 86% upon increasing resin concentration from 2000 to 4000 mg L^{-1}, whereas the corresponding removals achieved using the hybrid system featuring the epidermal-like structure resin were 61% and 73%, respectively. In particular, the boron removal of the hybrid system with the epidermal-like structure resin increased with increasing replacement rate of the virgin and saturated resins. Furthermore, the highest arsenic removal of 36% was achieved using the hybrid system with a gel-based resin concentration of 4000 mg L^{-1}. In addition, Kabay et al. used an ion-exchange resin (Dowex XUS-43594.00)–UF membrane hybrid system to decrease the concentration of boron in geothermal water samples to less than 1 mg L^{-1} utilizing adsorbent doses of 1000 or 1500 mg L^{-1}, a resin replacement rate of 3 or 6 mL min^{-1} and a permeate flow rate of 10 mL min^{-1} (Kabay et al., 2013).

Owing to silica scaling in pipelines, membranes, and heat exchangers, traditional drinking water treatment processes allow silica concentration of up to 150 mg L^{-1}, owing to the solubility of amorphous silica and silicates (Al-Rehaili, 2003). A continuous stirred tank reactor and an adsorbent–membrane hybrid system featuring iron oxy/-hydroxide agglomerates as the adsorbent and a hollow-fiber UF membrane (MWCO = 30,000 Da) were used to remove silica from brackish water (Shemer et al., 2019). The results suggested that a short residence period of ~15 min was adequate to reach the highest adsorption ability, which was comparable to that achieved during batch isotherm experiments. The adsorption capability of the hybrid system increased upon increasing silica concentration from 25 to 70 mg L^{-1} and decreased upon increasing adsorbent dosage from 200 to 1100 mg L^{-1}. The initial flux of the hybrid system quickly decreased by ~7% within 30 min, and it remained constant over the remaining 180 min of the experiment. This behavior was attributed to the decrease in concentration polarization during the early stages of cross-flow filtration (Sablani et al., 2001). In addition, because the water flux remained constant, the UF membrane did not foul in the presence of iron oxy/hydroxide agglomerates particles with a diameter of 22.6 μm (Shemer et al., 2019).

The presence of large amounts of phosphate anions in natural waters can cause cyanobacteria to bloom and discharge toxins, which are unsafe to the environment (Corbel et al., 2014). Hybrid systems comprising a submerged low-pressure UF membrane (hydrophilic polyether sulfone; MWCO = 200,000 Da) and granular ferric hydroxide and iron oxy/-hydroxide agglomerates as adsorbents were used to remove phosphate anions from synthetic secondary effluents (Hilbrandt et al., 2019). The 50% breakthrough (permeate concentration = 2 mg L^{-1}) of ferric hydroxide particles increased from 4 to 7.5 L g^{-1} and the 80% breakthrough increased from 10.5 to 16 L g^{-1}, corresponding to increases in the specific throughputs of approximately 85% and 50%, respectively. The specific throughputs increased by approximately 60% and 15% until the breakthroughs of the iron oxy/hydroxide agglomerates reached 50% and 80%, respectively. The presence of background Mg^{2+} (34 mg L^{-1}) and Ca^{2+} (86 mg L^{-1}) cations caused adsorbent saturation within <10 L g^{-1}. Significant electrostatic attraction can occur between the background cations and the negatively charged iron hydroxide surface (Li and Yang, 2016). Therefore, phosphate anion adsorption can be improved and ternary complexes probably form in the process (Wang et al., 2019). Moreover, background anions, including SO_4^{2-} (82 mg L^{-1}) and HCO_3^- (284 mg L^{-1}), can compete with the phosphate ions for adsorbent adsorption sites(Hilbrandt et al., 2019), whereas a separate study reported that the effect of SO_4^{2-} background anions on phosphate ion removal using iron hydroxide fine particles was negligible (Zelmanov and Semiat, 2015).

2.3. Adsorption–MF membrane hybrid systems

2.3.1. Organic compounds

NOM: The effect of inorganic/organic colloids and NOM on the decrease in the membrane flux of MF membranes with pore sizes in the range of 0.1–10 mm via fouling have been evaluated previously (Chen et al., 1997; Lee et al., 2006b). Fabris et al. used a magnetic ion-exchange resin and PAC as pretreatment adsorbents and flat-sheet

polyvinylidene difluoride (0.22 μm) and submerged hollow fiber (0.2 μm) as membrane materials to remove NOM from surface water (Fabris et al., 2007). High-performance size-exclusion chromatography analyses indicated that the flat-sheet MF membrane did not remove any NOM constituents with MWCOs in the range of 300–8000 Da, because the membrane pore size was much smaller than that of such constituents. Nevertheless, larger-molecular-weight NOM and colloids (MWCO >50, 000 Da) appeared to be the main short-term foulants. Most NOM, regardless of molecular weight, was successfully removed from water using magnetic ion-exchange resin–PAC–aluminum sulfate–MF membrane hybrid systems (Fabris et al., 2007).

Extracellular polymeric substances produced by bacteria, such as polysaccharides, proteins, lipids, and deoxyribonucleic acid, are large compounds (Barker and Stuckey, 1999). A decrease in hydraulic retention time enhanced biomass growth and soluble microbial product deposition, which increased membrane fouling degree (Huang et al., 2011). Khan et al. demonstrated and quantified the active effects of hydraulic retention time and various extracellular polymeric substances excreted by microorganisms on the performance of a submerged hollow-fiber polyethylene hydrophilic MF membrane (pore size = 0.1 μm) combined with PAC as the adsorbent in a membrane bioreactor for extended operation periods (45 d) (Khan et al., 2013). A previous study on a PAC–MF membrane hybrid system indicated that cake/gel layer development was the membrane fouling mechanism (Khan et al., 2011); however, this study did not report the formation of a thick cake layer on the external surface of any of the fouled membranes. This was ascribed to aeration considerably removing cake fouling in this system because the turbulence generated by aeration facilitated the constant removal of the foulants deposited on the membrane surfaces into the bulk phase of the membrane bioreactor (Chu and Li, 2005). Moreover, another finding suggested that the decrease in hydraulic retention time led to an increase in number of membrane cleaning steps and enhanced irreversible membrane fouling even when the aeration rate was doubled (Khan et al., 2013).

Lee et al. removed dissolved organic carbon and turbidity from secondary domestic wastewater using PAC adsorption and coagulation as pretreatment methods, followed by hollow-fiber polyethylene hydrophilic MF (pore size = 0.4 μm) (Lee et al., 2005). They reported that the system presented acceptable performance in terms of dissolved organic carbon retention with increasing PAC dose (25–250 mg L^{-1}). The highest dissolved organic carbon removal (up to ~75%) was observed for a PAC dose of 250 mg L^{-1}; however, the membrane permeate flux of the system with a PAC dose of 125 mg L^{-1} was higher than that of the system with a PAC dose of 250 mg L^{-1}. Furthermore, turbidity removal decreased with increasing PAC dose from 125 to 250 mg L^{-1}. Therefore, 125 mg L^{-1} was the optimal PAC dose for the PAC–MF membrane hybrid system. A rapid decrease in flux was observed during the early stages of membrane filtration, suggesting that membrane pores were blocked by organic matter. The slow decrease in membrane permeate during the later stages of membrane filtration was ascribed to the buildup of PAC particles onto the membrane surface. However, at the optimal PAC concentration of 125 mg L^{-1}, the initial quick decrease in permeate flux was diminished, indicating that the dissolved organic matter did not come into contact with the membrane surface, probably owing to the electrostatic repulsions between the negatively charged PAC particles and the dissolved organic carbon (Lee et al., 2005).

Endocrine-disrupting compounds and pharmaceuticals: Two membrane bioreactors using PAC as the adsorbent and flat-sheet MF and hollow-fiber UF membranes were used to remove ibuprofen, naproxen, diclofenac, trimethoprim, sulfamethoxazole, erythromycin, roxithromycin, carbamazepine, estrone, and 17α-ethinyl estradiol micropollutants (Alvarino et al., 2017). The COD and NO_3^- removals of both hybrid reactors were very high (>95%), and, in particular, NO_3^- removal was achieved only after PAC was added to the reactors. The removals of the target contaminants ranged between 40% and 99%, depending on compound properties. For example, the removals of carbamazepine and diclofenac, which are known to be recalcitrant to biological treatment, ranged between 0% and 30% (Joss et al., 2006). However, the removals of carbamazepine and diclofenac after the addition of PAC to the MF-based membrane bioreactor were significantly higher (>90% and >80%, respectively) (Alvarino et al., 2017). The attraction between carbamazepine and diclofenac micropollutants and PAC was proportional to their hydrophobicity, which was assessed using the distribution coefficient values (2.77 for carbamazepine and 1.55 for diclofenac at pH 7) (Jung et al., 2013b). A PAC dose of 250 mg L^{-1} was added to the hybrid reactor every 35 d, as suggested in the literature (Serrano et al., 2011), because the removal of carbamazepine and diclofenac decreased with increasing operation time owing to PAC saturation. The degree of saturation, which depended on the functional groups of the compounds, affected the overall compound charge (Nguyen et al., 2012). Therefore, the saturation of the selected compounds at pH 7 decreased as follows: negatively charged compounds (diclofenac, ibuprofen, sulfamethoxazole) > neutral compounds (carbamazepine, estrone, and 17α-ethinyl estradiol > positively charged compounds (trimethoprim) (Alvarino et al., 2017).

Dye chemicals: Methylene blue removal was optimized using three granular activate carbon samples as adsorbents in a fixed-bed column and a cellulose acetate MF membrane in the dead-end filtration mode (Askari et al., 2019). The effects of several operational parameters (initial solute concentration (10–60 mg L^{-1}), feed flowrate (0.5–1.5 L min^{-1}), bed length (10–30 cm), and filter type) on the methylene blue removal rate were examined using breakthrough analysis and response surface methods. Under optimal experimental conditions (C_o = 39.9 mg L^{-1}, flowrate = 1.15 L min^{-1}, bed length = 30 cm) the theoretically calculated removal rate was the highest (3.88 s^{-1}), and was 99% of the experimental value. During the first 100 s of operation, the removal rate of the hybrid system was approximately 65% and 30% greater than those achieved using the fixed-bed adsorption column and dead-end filtration cell, respectively (Askari et al., 2019). Jirankova et al. analyzed the removal of Ostazin red reactive dye using a PAC–hollow-fiber dead-end MF membrane hybrid system (Jirankova et al., 2007) and reported that adsorption on coal-based PAC is a promising removal method. Moreover, their results suggested that PAC did not act as a foulant for the membrane and the permeate flux was recovered readily after membrane cleaning; however, the process required approximately 7 d to reach equilibrium.

Toxic synthetic reactive dyes, which are more environmentally challenging than other types of dyes, cause significant environmental contamination and pose severe health risks to humans and animals (Forgacs et al., 2004). Lee et al. comprehensively evaluated the removal of Reactive Orange 16 and Reactive Black 5 dyes via coagulation (using aluminum sulfate), adsorption (using three types of PACs), and MF (using a submerged hollow-fiber hydrophilic polyethylene membrane with a pore size of 0.4 μm) and compared the results with those obtained using a coagulation–adsorption–MF hybrid treatment system (Lee et al., 2006a). The adsorbability and kinetics of Reactive Orange 16 were much higher and faster, respectively than those of Reactive Black 5. This was attributed to the properties of the dyes, because adsorption on PAC is typically favored for high-molecular-weight compounds with high aromaticity, low solubility, low polarity, and short carbon chains (Papic et al., 2004). The molar mass of Reactive Black 5 (991 g mol^{-1}) is higher than that of Reactive Orange 16 (617 g mol^{-1}); moreover, Reactive Black 5 contains more sulfonic acid functional groups than Reactive Orange 16, decreasing its adsorbability on PAC (Sarasa et al., 1998). When dye-containing wastewater was filtered using the MF membrane in the absence of the coagulant and/or adsorbents, membrane fouling was significant (~50% of the original permeate flux) and dye removal rate was very low (<3%) throughout the process (300 min) (Lee et al., 2006a). However, after coagulation/adsorption pretreatment, membrane efficiency increased (>95%) and the decrease in permeate flux was negligible (>1%; initial fluxes of 330 and 324 L h^{-1} m^{-2} for

Table 1
Summary of removal of contaminants in various adsorption-membrane hybrid systems.

Membrane class	Contaminant/ compound	Adsorbent/membrane	Experimental condition	Key removal/ performance	Key finding	Ref.
NF	Oleuropein	Imprinted polymers/ nanofiltration	Oleuropein in ethyl acetate; cross-flow system; adsorbent dose = 8 g	97.5% recovery (ethyl acetate solvent); 44.5% reduction (carbon footprint)	The very high selectivity of the imprinting technology resulted in the recovery of oleuropein with 99.7% purity at a rate of 1.75 g product per kg of adsorbent per hour.	Didaskalou et al. (2017)
	COD BOD Detergents	TiO_2, activated carbon/ polymeric membrane (polyacrylonitrile, polyvinylpyrrolidone, and dimethylformamide)	Municipal WW; cross-flow cell; C_o = 320, 190, 2.1 mg L^{-1} (COD, BOD, detergents); adsorbent dose = 2000 mg L^{-1}	92% (COD), 91% (BOD), 90% (detergents) in adsorption, photocatalyst, membrane hybrid system	Membrane filtration showed the best removal among single stage processes and the best removal performance was obtained when photocatalytic degradation, adsorption, and membrane filtration were employed in series, respectively.	Ejraei et al. (2019)
	COD dissolved organic carbon	Four PACs/NF PES010 (4 inch module, MWCO -1000 Da)	Sewage plant effluent; single element (pilot); C_o = 10–20 mg L^{-1} (COD); adsorbent dose = 500–1000 mg L^{-1}	20–45% (COD); 20–55% (dissolved organic carbon); >99% (color)	The particle layer could at least partially be removed by a flushing procedure consisting of a break of operation and a cross-flow recirculation without pressure.	Meier and Melin (2005)
	Total petroleum hydrocarbons	NaA zeolite nanoparticles modified by surfactant/cross-connection polyaniline membrane	Oil-filed WW; dead-end cell; C_o = 300 mg L^{-1}; adsorbent dose = 250–1250 mg L^{-1}; 5 bar	95.3–99.77% (temperature = 25–65 °C); permeate flux = 191 kg h^{-1} m^{-2}	Two combination of two adsorption and nanofiltration processes as well as the influence of NaA zeolite nanoparticles functioning as adsorbents, membrane deflation was minimized.	Esmaeili and Saremnia (2018)
	Bisphenol A	Iron(III)-tetrasulfophthalocyanine/ piperazine–polyamide (MWCO, 300 Da)	Synthetic water; cross-flow system; C_o = 2 mg L^{-1}; adsorbent dose = 300 mg L^{-1}	~75% (adsorbent + membrane); >99% (adsorbent + membrane + catalyst)	The prepared catalyst enhanced the bisphenol A removal (over 98% conversion within 1 h) in the presence of H_2O_2 at neutral pH.	Kim et al. (2008)
	Levofloxacin	Magnetic carbon nanocomposite/Dow Film Tec. (salt rejection, >97%)	Industry effluents; cross-flow system; adsorbent dose = 20, 40 mg L^{-1};	96% (NF); low (UF); 100% (RO)	In hybrid membrane processes enhanced permeate flow and percent removal of levofloxacin were observed in the presence of magnetic carbon nanocomposite.	Ullah et al. (2019)
	Rhodamine B crystal violet orange G indigo carmine	Multi-walled carbon nanotubes/polyethersulfone (pore diameter 0.73 nm)	Synthetic water; cross-flow system; C_o = 100 mg L^{-1}	99% (Rhodamine B); 98% (Crystal violet); 87% (Orange G); 82% (Indigo carmine)	Retention for the two cationic dyes was greater than 98% and for the two anionic dyes was greater than 82%.	Peydayesh et al. (2018)
UF	Bisphenol A 17β-estradiol	Single-walled carbon nanotubes/polyethersulfone, MWCOs (5,000, 10,000, and 30,000 Da)	Synthetic water; dead-end; C_o = 1 μM; adsorbent dose = 10 mg L^{-1}	20.2–62.8% (bisphenol A); 10.3–80.6% (17β-estradiol)	The percentage of bisphenol A and 17β-estradiol adsorption ranged from approximately 10 to 95% depending upon solution pH and the absence or presence of natural organic matter and Single-walled carbon nanotubes.	Heo et al. (2012a)
	Methyl green Lanasyn S	Mesoporous material (MCM-41)/polyvinyl chloride hollow fiber (overall pore size = 0.01–0.1 μm)	Synthetic/actual WW; hollow fiber module (batch/ semi-batch/single-pass); C_o = 10–50 mg L^{-1} ; adsorbent dose = 20 mg L^{-1}	Batch > semi-batch > single-pass (42.5 L h^{-1} m^{-2} and 94.8% batch full cycled)	Dye removal from actual WW more than 97% and permeate flux equal 39 L h^{-1} m^{-2} was obtained, showing that the hybrid system effectively removes dyes from both synthetic and actual WW.	Alardhi et al. (2020)
	Ten pharmaceuticals COD nitrification	PAC/MBR (0.045 μm pore size)	Synthetic water; hollow fiber membrane; C_o = 2.5 μg L^{-1}; adsorbent dose = 1–10 mg L^{-1}; 210 d	223 mg COD g_{vss}^{-1} d^{-1}; 25 mg N g_{vss}^{-1} d^{-1} (ammonia); 14 mg N g_{vss}^{-1} d^{-1} (nitrate)	The removal of diclofenac and roxithromycin might be related to the adsorption or biotransformation processes occurring in the cake layer.	Alvarino et al. (2017)
	COD dissolved organic carbon	CWZ30 PAC/polyacrylonitrile (MWCO, 110,000 Da)	Surface/lake water; cross-flow; C_o = 8–9 mg L^{-1}; adsorbent dose = 100 mg L^{-1}	92% (color); 63% (UVA 254); 65% (COD)	The role of PAC suspended in a feed in the PAC/UF system is the adsorption of low molecular organic compounds, which could not be removed by UF alone.	Mozia and Tomaszewska (2004)
	Bisphenol A 17α-ethinyl estradiol	Single-walled carbon nanotubes/ultrafiltration membrane MWCO (5000 Da)	Synthetic seawater; dead-end; C_o = 1 μM; adsorbent dose = 10 mg L^{-1}	77.3% (bisphenol A); 90% (17α-ethinyl estradiol)	UVA_{254} nm absorbance provides reasonable values as an alternative to total organic carbon analysis for highly aromaticity soil humic acid in synthetic seawater.	Heo et al. (2011)
	Diclofenac carbamazepine amoxicillin	PAC/hollow fiber (MWCO, 100,000 Da)	Synthetic water; submerged in a glass tube;	92–99% (decreased with increasing time)	Membrane alone insufficiently removes contaminants with approximately 10% efficiency.	Secondes et al. (2014)

(*continued on next page*)

Table 1 (*continued*)

Membrane class	Contaminant/compound	Adsorbent/membrane	Experimental condition	Key removal/performance	Key finding	Ref.
			adsorbent dose = 0.75–4.5 g m^{-2}		Addition of PAC enhanced removals to approximately 99%.	
	Arsenic boron	N-methyl-D-glucamine functionalized resins/hollow fiber	Saline geothermal water; C_o = 10 mg L^{-1} (boron), 100–200 μg L-1 (arsenic); adsorbent dose = 2000–4000 mg L^{-1}	61–95% (boron); 21–64% (arsenic)	Boron removal with g resin increased from 66% to 86% by doubling the resin concentration while the respective values found for expanded gel resin were 61% and 73%.	Cermikli et al. (2020)
	Boron	Powdered boron selective ion exchange resin/GE-Zenon ZeeWood®	Seawater; submerged membrane unit; C_o = 2 mg L^{-1}; adsorbent dose = 0, 500, 1000 mg L^{-1}	80% (20 min); 85% (>40 min); Q_p = 10–15 mL min^{-1}	The finding suggested that the power input and consumption of chemicals in sorption-membrane filtration hybrid process were smaller than in fixed ion exchange process.	Guler et al. (2011b)
		Ion exchange resin Dowex/GE-Zenon ZW-1 (pore diameter 0.04 μm)	Geothermal water; submerged membrane unit; C_o = 4.75–5.15 mg L^{-1}; adsorbent dose = 1000–1500 mg L^{-1}	~90–95% (20–60 min); ~85–90% (60–18040 min); Q_p = 10 mL min^{-1}	It appeared to reduce the boron concentration in the geothermal water to < 1.0 mg B/L where most crops are sensitive in irrigation water.	Kabay et al. (2013)
		Monodisperse nanoporous polymers/GE-Zenon ZW-1 (pore diameter 0.04 μm)	Geothermal water; submerged membrane unit; C_o = 10–11 mg L^{-1}; adsorbent dose = 2000–4000 mg L^{-1}	11.2, 14.0, and 17.0 mg g^{-1} resin depending on adsorbents	It is very difficult to use ground particles of commercially available boron selective ion exchange resins in the hybrid system for real applications.	Samatya et al. (2015)
	Silica	Iron oxy/hydroxide agglomerates; UFP-30-C-4A hollow fiber (MWCO, 30,000 Da)	Brackish water; continuous stirred tank ractor; C_o = 28–70 mg L^{-1}; adsorbent dose = 200–1100 mg L^{-1}	93% (60 mg L-1 silica, 67% recovery)	A short residence time of 15 min was necessary to obtain the maximum adsorption capacity similar to that achieved in batch isotherm experiments.	Shemer et al. (2019)
	Cd^{2+} Pb^{2+}	Aceh natural zeolite/polyethersulfone (MWCO, 20,000 Da)	Synthetic water; dead-end filtration; C_o = 20 mg L^{-1}; adsorbent dose = 1000 mg L^{-1}	78% (Pb); 85% (Cd)	The final concentration of Cd^{2+} was 0.21 mg L^{-1}, and 0.242 mg L^{-1} for Pb^{2+}. Even if the final concentrations were still somewhat above the permissible threshold.	Mulyati and Syawaliah (2018)
	NOM	PAC, iron oxide particles/polyethersulfone (MWCO = 100,000 Da)	Surface/river water; dead-end; C_o = 2.4–2.9 mg L^{-1}; adsorbent dose = 0–100 mg L^{-1} (Fe); pre-chlorination	~40% (w/pre-chlorination); ~30% (w/o pre-chlorination)	Iron oxide particles lower doses than PAC, though the sorption capacity of iron oxide particles declined slightly after chlorination of raw water.	Ha et al. (2004)
		Ferrihydrite, PAC/regenerated cellulose ultrafilters (MWCOs, 10, 30, and 100,000 Da)	Surface/lake water; dead-end; C_o = 4.8 mg L^{-1}; adsorbent dose = 0–500 mg m^{-2}	32–49% (100 kDa, ferrihydrite); 70% (30 kDa, ferrihydrite)	The data of hydraulic filtration resistance indicated that adsorbents played a role in decreasing reversible fouling caused by the deposition of NOM on the membrane surface.	Kang and Choo (2010)
		Heated aluminum oxide particles/polyethersulfone (pore size 0.05 μm)	Freshwater and seawater; dead-end; C_o = 1.4–2.3 mg L^{-1}; adsorbent dose = 18 g L^{-1}	40–50% (based on dissolved organic carbon); 50–70% (based on UVA_{254})	The heated aluminum oxide particles layer imposes very low hydraulic resistance, but it is capable of adsorbing NOM, including foulant molecules.	Kim et al. (2010)
	Humic acid	Oxygen-/nitrogen-based activated biochar/polyethersulfone (MWCO, 5000 Da)	Synthetic water; dead-end cell; C_o = 5 mg L^{-1}; adsorbent dose = 20–40 mg L^{-1}	~85–95% (N-biochar > O-biochar > PAC); 38.1% (irreversible fouling rate decrease)	N-activated biochar showed significantly stronger π-π interactions, more polar functional groups, and greater inner pore sites than PAC or O-activated biochar.	Chu et al. (2017)
		Single-walled carbon nanotubes/ultrafiltration membrane MWCO (10,000 Da)	Synthetic water; dead-end; C_o = 8 mg L^{-1}; adsorbent dose = 20, 50 mg L^{-1}	~75–85% (UVA); ~70–75% (total organic carbon)	The use of single-walled carbon nanotubes to control membrane fouling appears to be a function of hydrodynamic and operational conditions.	Heo et al. (2012b)
		PAC/polyethersulfone (MWCO, 100,000 Da)	Synthetic water; dead-end; C_o = 10 mg L^{-1}; adsorbent dose = 0–200 mg L^{-1}	40–55% (w/o Ca^{2+}); 80–95% (w/Ca^{2+})	PAC and humic acid showed an important synergistic effect when they formed a fouling cake together during the filtration regardless of the presence or absence of calcium.	Shao et al. (2016)
	Humic acid bovine serum albumin sodium alginate	Mesoporous adsorbent resin/polyethersulfone, cellulose acetate (MWCOs, 100,000 Da)	Two surface river waters; C_o = 1–30 mg L^{-1}; adsorbent dose = 50 mg L^{-1}	Humic acid > bovine serum albumin > sodium alginate	The effectiveness of adsorption pretreatment in NOM fouling control was associated with the characteristics of NOM and adsorbent.	Li et al. (2014)

(*continued on next page*)

Table 1 (*continued*)

Membrane class	Contaminant/compound	Adsorbent/membrane	Experimental condition	Key removal/performance	Key finding	Ref.
				(mesoporous adsorbent resin)		
		Ferrihydrite, PAC/polyvinylidene fluoride hollow fiber (pore size, 0.02 μm)	Synthetic water; submerged system; C_o = 5 mg L^{-1}; adsorbent dose = 12.5–150 mg L^{-1}	91.6% (ferrihydrite); 66.6% (PAC)	The adsorption capacities of ferrihydrite for different dissolved organic fractions were in the order of humic acid > bovine serum albumin > sodium alginate.	Zhang et al. (2018)
	Heavy crude oil	Magnetic inorganic-organic hybrid powder and polyethersulfone membrane	Spilled heavy crude oil; C_o = 2–4 g L^{-1}; adsorbent dose = 40–60 mg with a contact time of 2 min	>95% (crude oil = <3.5 g); 60–95% (crude oil = 3.5–5 g)	The use of the magnetic hybrids fabricated using biomass wastes, together with the hybrid magnetic membrane, showed an effective and inexpensive technological alternative for the removal of oil from water surfaces.	Cunha et al. (2019)
	Phosphate	Fine iron hydroxides particles/polyether sulfone-polyethylene terephthalate (200 Da)	Synthetic secondary effluent; submerged system; C_o = 10 mg L^{-1} P; adsorbent dose = 20–300 mg L^{-1} Fe	50% breakthrough (15 L g^{-1} Fe); 50% higher in secondary effluent than that in deionized water	For both adsorbents phosphate adsorption increased with the decrease of pH. While, the iron hydroxides showed 30–50% higher loadings compared to granular ferric hydroxide.	Hilbrandt et al. (2019)
	Phenol	Hypercrosslinked polymers/ZW-1 model (GE, pore size 0.04 μm)	Synthetic water; submerged system; C_o = 50 mg L^{-1}; adsorbent dose = 1000–4000 mg L^{-1} Fe	~90% (Q_{feed} – 5 mL min^{-1}); ~95% (Q_{feed} – 3 mL min^{-1})	Optimum amount of adsorbent appeared to be 0.1 g-adsorbent/50 mL-solution and 0.2 g-adsorbent/50 mL-solution for Purolite MN 200 and Purolite MN 202, respectively.	Ipek et al. (2012)
	Phenol chlorophenol, nitrophenol hydroquinone	Magnetic PAC/polyethersulfone (MWCO, 100,000 Da)	Synthetic water; dead-end filtration; C_o = 40–50 mg L^{-1}; adsorbent dose = 10 mg L^{-1} Fe	103, 217, 141, 730 mg g^{-1}, phenol, nitrophenol, chlorophenol, Hydroquinone, respectively	The problems associated with PAC in the UF processes such as cake formation and blackening of the pipes were not observed for magnetic PAC.	Zahoor and Mahramanlioglu (2011)
	Ibuprofen 17 α-ethinyl estradiol carbamazepine	Activated biochar, PAC/polyamide thin film composite (MWCO, 3000 Da)	Synthetic water; dead-end filtration; C_o = 10 μM; adsorbent dose = 10 mg L^{-1}	24–37% (w/humic acid); 41–53% (w/o humic acid; ibuprofen >17 α-ethinyl estradiol > carbamazepine	The governing mechanism of removal in the UF-activated biochar system is hydrophobic interaction (adsorption) between the compounds and activated biochar.	Kim et al. (2019)
	Diclofenac	Special iron-impregnated PAC/hollow fiber UF	Synthetic water; submerged system; C_o = 0.5–1 mg L^{-1}; adsorbent dose = 10–50 mg L^{-1}	117 mg g-1; 70% (PAC; 77.6% (iron-impregnated PAC)	The impregnation of iron nanoparticles (ferrihydrite) into the carbon surface could enhance the decomposition of H_2O_2 to strong hydroxyl species, improving the regeneration effectiveness of the composite adsorbent.	Sarasidis et al. (2017)
	Methylene blue methyl orange	$Ti_3C_2T_x$ MXene, PAC/polyamide thin film composite (MWCO, 3000 Da)	Synthetic water; dead-end filtration; C_o = 2 mg L^{-1}; adsorbent dose = 20, 50, and 100 mg L^{-1}	80, 91, and 99% (MXene-UF); 86, 92, and 99.5% (PAC-UF)	Dyes can be adsorbed onto MXene, and only small amounts of MXene are deposited on the filtration membrane due to electrostatic repulsion.	Kim et al. (2020b)
	Ibuprofen 17α-ethinyl estradiol humic acid tannic acid	Metal-organic frameworks (MIL-100(Fe) and MIL-101 (Cr))/polyamide thin film composite (MWCO, 3000 Da)	Synthetic water; dead-end filtration; C_o = 10 μM (ibuprofen 17α-ethinyl estradiol), 10 mg L^{-1}; adsorbent dose = 20 mg L^{-1}	23–70% (ibuprofen), 32–62% (17α-ethinyl estradiol)- MIL-100 (Fe); 24–71% (ibuprofen), 45–72% (17α-ethinyl estradiol)- MIL-101(Cr)	MIL-101(Cr), with larger inner pores, showed greater solution stability than MIL-100(Fe), resulting in a greater pharmaceutical removal rate.	Kim et al. (2020a)
MF	Cd Hg Ni Co Pb	Multi-walled carbon nnanotubes/0.2 μm ceramic membrane	Synthetic water; placed in a stainless steel housing; C_o = 100 mg L^{-1}; adsorbent dose = 10 mg L^{-1}; 3 d	>95% (general hydrocarbons); >93% (Cd, Hg, Ni, Co and Pb); regenerated with 50:50 acetic acid:water	The basic chemical analysis conducted onsite indicates that the permeate supply generated was free from microbial contamination and the flux rates were around 33% of the clean water flux achieved in the laboratory.	Ainscough et al. (2017)
	Ten pharmaceuticals COD nitrification	PAC/MBR (0.45 μm pore size)	Synthetic water; flat sheet membrane; C_o = 2.5 μg L^{-1}; adsorbent dose = 1–10 mg L^{-1}; 210 d	220 mg COD g_{vss}^{-1} d^{-1}; 24 mg N g_{vss}^{-1} d^{-1} (ammonia); 7 mg N g_{vss}^{-1} d^{-1} (nitrate)	The degree of removal by PAC could be related to the log D of the compound, while the saturation of PAC depended on the ionic charge of the organic micropollutants.	Alvarino et al. (2017)
	Disinfection by-products	Ferrihydrit amorphous iron oxide/polyvinylidene fluoride (pore size 0.1 μm)	Surface water; dead-end system; C_o = 420 μg L^{-1};	Approximately 30% (total) depending on eight different	Disinfection by-products formation potential in ferrihydrit -treated waters	Osawa et al. (2017)

(*continued on next page*)

Table 1 (*continued*)

Membrane class	Contaminant/compound	Adsorbent/membrane	Experimental condition	Key removal/performance	Key finding	Ref.
			adsorbent dose = 1700 mg L^{-1}	disinfection by-products	is mostly smaller than that in PAC-treated waters.	
	Methylene blue	Peach-core-based GAC/QS 100–1000 (pore diameter 2–5 μm)	Synthetic water; fixed-bed column; dead-end depth filtration; C_o = 20–60 mg L^{-1}; bed length = 10–30 cm	Maximum removal rate = 3.785 s^{-1} @ C_o = 40 mg L^{-1}; bed length = 30 cm; flowrate = 1.15 L min^{-1}	The removal rate achieved with the hybrid process was approximately 65% greater than that achieved with the fixed-bed adsorption column and 30% greater than that achieved with the dead-end depth cell.	Askari et al. (2019)
	Ni	Surfactant-added PAC/cellulose acetate; cellulose nitrate; mixed cellulose ester (0.2–0.45 μm)	Synthetic water; cross-flow cell; C_o = 10–300 mg L^{-1}; adsorbent dose = 100–4000 mg L^{-1}	Removal = 2 times higher; flux decline = 10 times greater	Surfactant type and membrane pore size were established as having the highest and the lowest total impact on process performance, respectively	Aydiner et al. (2006)
	CrO_4	Surfactant-added PAC/MF	Synthetic water; cross-flow cell; C_o = 0.2–5 mM; surfactant = 0.2–0.8 mM; adsorbent dose = 500–2000 mg L^{-1}	Cetyl trimethyl ammonium bromide (91%); CrO_4^{2-} (97.2%) @ PAC (500 mg L^{-1}) and surfactant = 5 mM	Rejections and fouling in membrane were shown as a dynamic function of PAC, cetyl trimethyl ammonium bromide and CrO_4^{2-} as the properties of the feed solution.	Basar et al. (2006)
	Rubidium	Potassium cobalt hexacyanoferrate/hollow fiber membrane (pore size 0.1 μm)	Synthetic seawater; submerged system; C_o = 5 mg L^{-1}; adsorbent dose = 50, 100, and 2000 mg L^{-1}	95% (0–1 h); 93–96% (1–26 h); 142 mg (24 mg g^{-1}) for adsorption only	The adsorption capacity of potassium cobalt hexacyanoferrate was reduced by only 33% in synthetic seawater containing high concentrations of Na, K, Ca, and Mg compared to Rb-only solution.	Nur et al. (2018)
	NOM	Heated aluminum oxide particles/polyethersulfone (pore size 0.05 μm)	Lake water; dead-end cell; C_o = 0.2–5 mM; adsorbent dose = 0.052 mmol cm^{-2} as Al^{3+}	Removal increased up to 10–20 times as much NOM as when no adsorbents were added.	Pre-deposition of 5 mg L^{-1} adsorbent (as Al^{3+}) allowed the system to operate 5 times as long before the transmembrane pressure increased by 6.9 kPa.	Cai et al. (2008)
		MIEX®/polyvinylidene difluoride (0.22 μm), hollow fiber (0. 2 μm)	Surface water; dead-end cell/submerged; C_o = 2.2/11.7 mg L^{-1}; adsorbent dose = 10 mL L^{-1}	Both reversible and irreversible resistance = 21.5–46.4%	Treatments that removed most of the dissolved organic matter but did not remove the colloidal components, were unable to avoid fouling.	Fabris et al. (2007)
		PAC/hollow fiber (polyethylene hydrophilic, 0.1 μm)	River & biofiltered water; submerged; C_o = 2–3 mg L^{-1}	97% (polysaccharides); >95% (proteins)	The hydraulic retention time is one of the most important parameters during system (PAC-MF membrane bioreactor) design.	Khan et al. (2013)
	Total organic carbon turbidity	Wood/coal/coconut based PACs/hollow fiber (polyethylene hydrophilic, 0.4 μm)	Secondary domestic WW; submerged; C_o = 4.6 mg L^{-1}; adsorbent dose = 25–250 mg L^{-1}	57% (wood); 48% (coal); 70% (coconut)	When WW alone was introduced into MF system without coagulation, fouling of the membrane was severe by decreasing nearly 80% of the initial permeate flux within 1 h of operation.	Lee et al. (2005)
	COD, Ni, Cr, Cu, and Zn	GAC/aluminum oxide ceramic membrane (pore size 0.1 μm)	Metal-plating WW; flat-tubular; C_o = 463 mg L^{-1}; packing ratio = 10 and 30%	80–85% overall Removal = pH 7 > pH 2	Low COD removal efficiency was achieved regardless of the pH change in wastewater without fluidized media.	Chang et al. (2020)
		Coagulation-PAC/polyvinylidene fluoride flat sheet (pore size 0.22 μm)	Concentrated municipal WW; dead-end cell; C_o = 10,837 mg L^{-1}	20.8 × 10^{10} m^{-1} (reduced irreversible fouling); 7.04 × 10^{10} m^{-1} (no cake layer existed)	The finding showed outstanding reduced irreversible membrane fouling caused by adsorbent cake layer existence during concentration of raw sewage organic matter through dead-end filtration cell.	Gong et al. (2017)
	Organic dyes	Coal-based PAC/polypropylene hollow fiber (pore size 0. 1 μm × 0.7 μm)	Industrial WW; submerged system; C_o = 34 mg L^{-1}; adsorbent dose = 3000 mg L^{-1}	>95% (10–100 min); ~55–95% (100–450 min)	There is insignificant resistance caused by the cake, as the PAC cake was fairly loosely adhered to the membrane surface.	Jirankova et al. (2007)
	Bemacid Red E-TL	Diatomaceous marl/alumina ceramic MF (pore size 0.1 μm)	Synthetic Industrial WW; tubular system; C_o = 1,000 mg L^{-1}; adsorbent dose = 500–3000 mg L^{-1}	Water permeance of 380–420 L m^{-2} h^{-1} bar^{-1}	The crystalline phases are, in descending order of importance, Calcite, Quartz, calcium magnesium iron carbonate and a phyllosilicate phase identified as been Muscovite.	Maimoun et al. (2020)
	Black 5 Orange 16 Nitrate	Wood/coal/coconut based PACs/hollow fiber (polyethylene hydrophilic, 0.4 μm)	Synthetic WW; submerged; C_o = 100–250 mg L^{-1}; adsorbent dose = 125–250 mg L^{-1}	99.9% (350 mg L^{-1} coagulant + 200 mg L^{-1} PAC for Orange 16)	Adsorption capacity of Orange 16 was much greater and quicker than those of Black 5 due to the different molecular dimension, solubility and surface functional groups.	Lee et al. (2006a)

(*continued on next page*)

Reactive Black 5 and Reactive Orange 16, respectively) throughout the experiment (300 min).

2.3.2. Inorganic compounds

Cationic heavy metal contaminants: Wastewater from the metal-plating industry is typically strongly acidic and contains high levels of inorganics, organics, and particulates (Katsumata et al., 2003). A submerged aluminum oxide ceramic MF membrane (pore size = 0.1 μm) combined with fluidized granular activated carbon as the adsorbent was used to treat actual hazardous metal-plating industry wastewater samples (pH 2, COD = 463 mg L^{-1}, total suspended solids = 102 mg L^{-1}, Ni = 186 mg L^{-1}, Cr = 332 mg L^{-1}, Cu = 51 mg L^{-1}, and Zn = 4.2 mg L^{-1}) (Chang et al., 2020). Raw wastewater neutralization caused particle and colloid aggregation (average aggregate size increased from 10.1 μm at pH 2–28.7 μm at pH 7), resulting in a significant decrease in membrane flux owing to fouling at the membrane surface. At the raw wastewater pH of 2, the aluminum oxide ceramic membrane with a point of zero charge of 5.4 (Gulicovski et al., 2008) became negatively charged; therefore, heavy metal cations were repelled by the membrane surface. However, at pH 7, charge neutralization led to an increase in suspended solid concentration from ~100 to 450 mg L^{-1} owing to aggregate formation and particle and colloid precipitation. Membrane pressure increased quickly at pH 7; however, the removal efficiencies of the membrane for Ni, Cr, Cu, and Zn ions were high (81%, 59%, 48%, and 98%, respectively). At pH 2, the fluidized adsorbent–ceramic MF membrane hybrid system did not remove any heavy metals. The increase in heavy metal removal efficiency at higher solution pH was attributed to the formation of abundant metal–organic particulate complexes, which can be readily removed by the membrane (Nedzarek et al., 2015). Additionally, the cake layer formed by the total suspended solids in raw wastewater on the membrane surface can act as a secondary membrane to increase the heavy metal ion removal rates of the membrane (Ahmad et al., 2018).

A new adsorption–membrane hybrid system comprising functionalized multi-walled carbon nanotubes as the adsorbent and a super hydrophilic ceramic membrane (pore size = 0.2 μm) exhibited minimal membrane fouling during Hg, Cd, Co, Ni, and Pb removal from severely contaminated river water (Ainscough et al., 2017). The membrane presented an initial high permeability (~1400 L m^{-2} h^{-1} bar^{-1}) for clean water; however, its fast flux for a highly contaminated feed water sample containing used engine oil decreased to approximately 100 L m^{-2} h^{-1} bar^{-1} and did not change over a long period (10 d). The removal capacity of MF membranes with small pore size is predictable, i.e. microbials are readily rejected. The removal rates of the adsorbent for the target heavy metals and hydrocarbons were very high (99.3% and 99.5%, respectively); moreover, the adsorbent was easily regenerated using an aqueous acetic acid solution (50% w/v), and the regenerated adsorbent presented almost the same removal rates as the fresh adsorbent (Ainscough et al., 2017). In a separate study, used a surfactant-enhanced PAC–MF membrane hybrid system for Ni removal. The removal capacity of the system increased when the surfactant concentration was higher than the critical micellar concentration, owing to the enhanced steric effects associated with the additional membrane layer formed by the surfactant on the surface and inside the pores of the membrane (Aydiner et al., 2006). Although the membrane flux varied significantly with the surfactant type and concentration and membrane material and pore size, a significant decrease in the steady-state flux of the system was observed, which was a major disadvantage.

Anionic heavy metal contaminants: Toxic chromate (CrO_4^{2-}) anions were removed from synthetic solutions using an adsorbent–cross-flow MF membrane hybrid system featuring cationic surfactant (cetyl trimethyl ammonium bromide)-enhanced PAC as the adsorbent (Basar

Table 1 (*continued*)

Membrane class	Contaminant/compound	Adsorbent/membrane	Experimental condition	Key removal/performance	Key finding	Ref.
		Four ion exchange resins and two bio-adsorbents/modified poly acrylic nitrile hollow fiber (0. 1 μm)	Synthetic water; submerged system; C_o = 20 mg L^{-1}; adsorbent dose = 500 mg L^{-1}	60–80%; 50–80% (w/chloride); 60–75% (w/phosphate)	The material cost for the removal of 1000 mg of nitrate as N was 2.52, 3.81, 0.72 and 0.96 USD for Dowex-Fe, Dowex, AG coconut copra and AG corn cob, respectively.	Kalaruban et al. (2018)
	Arsenate	By-products from conventional iron oxyhydroxides/polyvinylidene difluoride (0.1 μm)	Synthetic groundwater; submerged system; C_o = 190 μg L^{-1}; adsorbent dose = 100 mg L^{-1}	80% (5 min); 70% (7 h)	As(V) adsorbent capacity in the hybrid system for As(V) increased and had nearly double when the As(V) feed concentration increased to 380 μg L^{-1} from 190 μg L^{-1} at lower hydraulic retention time.	Usman et al. (2021)
	Cesium	Copper ferrocyanide/mixed cellulose ester (pore size 0.22 μm)	Synthetic water; flat-sheet system; C_o = 99.1 μg L^{-1}; adsorbent dose = 40–250 mg L^{-1}	99%; after physical washing 84.4% recovered	The decontamination performance of the adsorption–coagulation–MF hybrid process was not significantly influenced by coagulation with Al^{3+} in the local tap water.	Xu et al. (2017)
	Boron	Powdered boron selective ion exchange resin/polypropylene hollow fiber (pore size 0. 4 μm)	Seawater; submerged membrane unit; C_o = 2 mg L^{-1}; adsorbent dose = 0, 500, 1000 mg L^{-1}	50% (5 min); 90% (40 min); Q_p = 2 mL min^{-1} (long-term study)	Boron concentration in product water was constant for long time operation in sorption-membrane hybrid system during 24 h of operation for suspension resin concentration of 1000 mg L^{-1}.	(Guler et al., 2011b)
		Microparticulate boron adsorbent Dowex XUS/ceramic MF (pore size 0.1 μm)	Synthetic water; tubular system; pH 0.5–13.5; minimum suspension volume = 3 dm^3	Optimum velocity = 2 m s^{-1}; 43 dm^{-3} m^{-2} h^{-1} at 20% mass dry adsorbent	From analysis of the flux decline by the modified Hermia model suggests that the dominant membrane fouling mechanism is a cake formation.	Onderkova et al. (2009)
		Microparticulate adsorbent 22/GE Zenon; ceramic membrane Membralox	Synthetic water; submerged/cross-flow cell; GE Zeono (40 kPa); ceramic membrane Membralox (41.5 kPa)	Optimum dry adsorbent = 110 kg m^{-3} (GE Zeono); 200 kg m^{-3} (ceramic membrane Membralox)	Specific consumption of regeneration media per unit volume of raffinate at these conditions are 0.97 and 0.19 mol m^{-3} for acid and alkali, respectively.	Blahusiak and Schlosser (2009)

WW = wastewater; GAC = granular activated carbon.

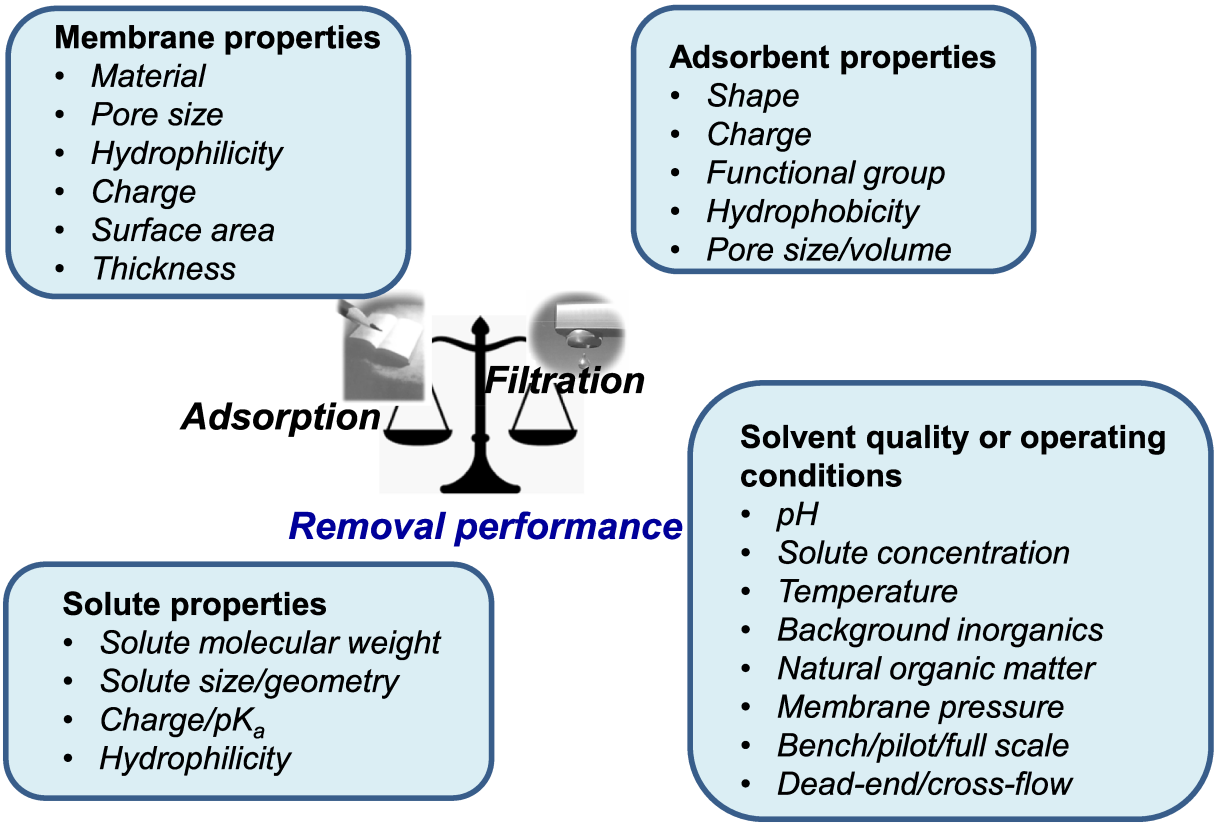

Fig. 6. Areas of future study of adsorbent-membrane hybrid systems for the removal of contaminants in aqueous solution.

et al., 2006). The removal and total resistance against membrane flux of the hybrid system increased with increasing surfactant concentration from 0.2 to 5 mM. Surfactant and chromate anion removal were lower at concentrations lower than the critical micellar concentration, than at concentrations higher than the critical micellar concentration. This was attributed to the development of various surfactant aggregates, such as bilayers, hemi-micelles, and micelle-like structures, in the feed phase. The main removal mechanisms consisted of the interactions of monomeric surfactants and aggregates with PAC at surfactant concentrations higher and lower, respectively, than the critical micellar concentration. Because large micelles cannot pass through the membrane owing to the formation of a secondary membrane at the surface and inside the pores of the cross-flow MF membrane surface (Basar et al., 2004), the increase in surfactant and chromate ion removal at concentrations higher than the critical micellar concentration was attributed to the formation of the secondary membrane. In addition, the formation of the secondary membrane led to a decrease in total membrane resistance and membrane permeate flux. chromate ion removal exceeded surfactant removal, particularly at concentrations lower than the critical micellar concentration, owing to the strong interaction between the chromate ions and amphiphilic surfactant aggregates attached to PAC, which was termed "adsolubilization" in a previous study (Talbot et al., 2003). Therefore, the adsorption and adsolubilization of chromate ions using surfactant-enhanced PAC is more dominant to reach decent surfactant and chromate removals than that of monomeric surfactants (Basar et al., 2006).

Adsorbent–membrane hybrid systems featuring a modified polyacrylonitrile hollow-fiber submerged MF membrane (pore size = 0.1 μm) and two ion-exchange resins and two chemically available bio-adsorbents were used to remove NO_3^- ions (Kalaruban et al., 2018). Transmembrane pressure increased with increasing operation time for all adsorbents. In particular, once the membrane treated more water with high flux, it appeared to have increased membrane fouling. Transmembrane pressure in the presence of bio-adsorbents in suspension was higher than that in the presence of ion-exchange resins, because the specific volumes of the ion-exchange resin and bio-adsorbents were high (0.9 and 1.1 $m^3\ kg^{-1}$, respectively). Therefore, relatively small-sized bio-adsorbents (300–600 μm) could have clogged a larger portion of the membrane surface than similar-sized ion-exchange resins, leading to an increase in transmembrane pressure. In addition, the small particles generated during bio-adsorbent grinding could clog the membrane because they can deposit between adjacent membrane layers (Kalaruban et al., 2018). Usman et al. comprehensively analyzed the removal of arsenate (AsO_4^{3-}) ions using an adsorbent–membrane hybrid system with two iron oxyhydroxide-based adsorbents (microgranular ferric hydroxide and microgranular manganese(IV) feroxyhyte) and a polyvinylidene difluoride MF membrane (pore size = 0.1 μm) (Usman et al., 2021). The results of a 6-h adsorption kinetics experiment indicated that the adsorption of arsenate ions on manganese(IV) feroxyhyte occurred faster than on ferric hydroxide. The hydraulic residence time and air bubbling rate of arsenate ions in the slurry reactor played significant roles in the performance of the hybrid system. The observed adsorption capacities of manganese(IV) feroxyhyte and ferric hydroxide increased with increasing residence times and air bubbling rates. In particular, at a relatively short hydraulic residence time of approximately 3 h, the volume of arsenate ion-containing water treated with manganese(IV) feroxyhyte was approximately 1.5 times large than that treated with ferric hydroxide under optimal experimental conditions (adsorbent dose = 1000 mg L^{-1}, membrane flux = 20 L $m^{-2}\ h^{-1}$, and pH 7). This was attributed to the kinetics of the adsorption reaction on manganese(IV) feroxyhyte being faster than on ferric hydroxide (Usman et al., 2021). The removal efficiencies of several adsorption–membrane hybrid systems for different contaminants and water samples under various experimental conditions are summarized in Table 1.

3. Conclusions and future research areas

Overall, previous studies have shown that adsorbent–NF/UF/MF membrane hybrid systems can be used to effectively remove numerous inorganic and organic contaminants from water. To date, PAC–membrane hybrid systems have been widely used; however, recent papers have described the use of different/new types of adsorbents, such as zeolite nanoparticles, magnetic carbon nanocomposites, carbon nanotubes, metal–organic frameworks, MXenes, N-methyl-D-glucamine–functionalized resins, iron oxy/hydroxide agglomerates, fine iron hydroxide particles, and potassium cobalt hexacyanoferrate particles, in adsorbent–membrane hybrid systems. Although previous studies have been focused mainly on the removal of NOM, COD, BOD, and total suspended solids from surface water and wastewater, the efficiency of adsorbent–membrane hybrid systems in the removal of contaminants of emerging concern (*e.g.,* endocrine-disrupting compounds and pharmaceuticals), dye chemicals, heavy metals, and toxic inorganics has recently been reported. In addition, previously published papers have indicated that the removal efficiency of adsorbent–membrane hybrid systems significantly varied and depended on the physicochemical properties of the contaminants, water quality parameters, adsorbent properties, and membrane properties and operating conditions.

However, most studies performed to date used only a few membrane types (NF, UF, or MF), focused on bench-scale experiments, or analyzed a limited number of contaminants under partial solution pH and background solute concentrations and operational conditions. In particular, only a few studies have evaluated the transport of contaminants at the pilot scale even with conventional parameters such as COD and dissolved organic matter. Therefore, a comprehensive evaluation of the removal of various conventional/emerging inorganic/organic contaminants is critical, particularly at pilot scale. This would allow measurement of large-scale and long-lasting membrane strength for supporting applications of adsorbent–membrane hybrid processes. Data from pilot-scale experiments should be relevant under environmentally relevant conditions, because the overall performance and hydraulics of membranes used for large-scale experiments are different from those of membranes used for bench-scale experiments. Fig. 6 illustrates the areas of future research of adsorption-membrane hybrid systems in terms of adsorbent/membrane properties, solute physicochemical properties, operation conditions, and solvent/water chemistry conditions in water.

Declaration of competing interest

The authors declare that they have no known competing financial interests or personal relationships that could have appeared to influence the work reported in this paper.

Acknowledgements

This research was supported by the National Science Foundation, USA (OIA-1632824). This work was also supported by the National Research Foundation of Korea (NRF) grant funded by the Korea government (MSIT) (No. NRF-2020R1A2C2100892).

References

Adak, A., Bandyopadhyay, M., Pal, A., 2005. Removal of anionic surfactant from wastewater by alumina: a case study. Colloids Surf., A 254 (1–3), 165–171.
Aguilar-Arteaga, K., Rodriguez, J.A., Barrado, E., 2010. Magnetic solids in analytical chemistry: a review. Anal. Chim. Acta 674 (2), 157–165.
Ahmad, R., Aslam, M., Park, E., Chang, S., Kwon, D., Kim, J., 2018. Submerged low-cost pyrophyllite ceramic membrane filtration combined with GAC as fluidized particles for industrial wastewater treatment. Chemosphere 206, 784–792.
Ainscough, T.J., Alagappan, P., Oatley-Radcliffe, D.L., Barron, A.R., 2017. A hybrid super hydrophilic ceramic membrane and carbon nanotube adsorption process for clean water production and heavy metal removal and recovery in remote locations. J. Water Process Eng. 19, 220–230.
Al-Rehaili, A.M., 2003. Comparative chemical clarification for silica removal from RO groundwater feed. Desalination 159 (1), 21–31.
Al-Rifai, J.H., Khabbaz, H., Schafer, A.I., 2011. Removal of pharmaceuticals and endocrine disrupting compounds in a water recycling process using reverse osmosis systems. Separ. Purif. Technol. 77 (1), 60–67.
Alardhi, S.M., Albayati, T.M., Alrubaye, J.M., 2020. A hybrid adsorption membrane process for removal of dye from synthetic and actual wastewater. Chem. Eng. Process 157, 108113.
Aloma, I., Martin-Lara, M.A., Rodriguez, I.L., Blazquez, G., Calero, M., 2012. Removal of nickel (II) ions from aqueous solutions by biosorption on sugarcane bagasse. J. Taiwan. Inst. Chem. E. 43 (2), 275–281.
Alvarino, T., Torregrosa, N., Omil, F., Lema, J.M., Suarez, S., 2017. Assessing the feasibility of two hybrid MBR systems using PAC for removing macro and micropollutants. J. Environ. Manag. 203, 831–837.
Askari, M., Salehi, E., Ebrahimi, M., Barati, A., 2019. Application of breakthrough curve analysis and response surface methodology for optimization of a hybrid separation system consisting of fixed-bed column adsorption and dead-end depth filtration. Chem. Eng. Process 143, 107594.
Aydiner, C., Bayramoglu, M., Kara, S., Keskinler, B., Ince, O., 2006. Nickel removal from waters using surfactant-enhanced hybrid PAC/MF process. I. The influence of system-component variables. Ind. Eng. Chem. Res. 45 (11), 3926–3933.
Barker, D.J., Stuckey, D.C., 1999. A review of soluble microbial products (SMP) in wastewater treatment systems. Water Res. 33 (14), 3063–3082.
Basar, C.A., Aydiner, C., Kara, S., Keskinler, B., 2006. Removal of CrO_4 anions from waters using surfactant enhanced hybrid PAC/MF process. Separ. Purif. Technol. 48 (3), 270–280.
Basar, C.A., Karagunduz, A., Cakici, A., Keskinler, B., 2004. Removal of surfactants by powered activated carbon and microfiltration. Water Res. 38 (8), 2117–2124.
Blahusiak, M., Schlosser, S., 2009. Simulation of the adsorption-microfiltration process for boron removal from RO permeate. Desalination 241 (1–3), 156–166.
Cai, Z.X., Kim, J.S., Benjamin, M.M., 2008. NOM removal by adsorption and membrane filtration using heated aluminum oxide particles. Environ. Sci. Technol. 42 (2), 619–623.
Carolin, C.F., Kumar, P.S., Saravanan, A., Joshiba, G.J., Naushad, M., 2017. Efficient techniques for the removal of toxic heavy metals from aquatic environment: a review. J. Environ. Chem. Eng. 5 (3), 2782–2799.
Cermikli, E., Sen, F., Altiok, E., Wolska, J., Cyganowski, P., Kabay, N., Bryjak, M., Arda, M., Yuksel, M., 2020. Performances of novel chelating ion exchange resins for boron and arsenic removal from saline geothermal water using adsorption-membrane filtration hybrid process. Desalination 491, 114504.
Chang, S., Ahmad, R., Kwon, D.E., Kim, J., 2020. Hybrid ceramic membrane reactor combined with fluidized adsorbents and scouring agents for hazardous metal-plating wastewater treatment. J. Hazard Mater. 388, 121777.
Chen, J., Chen, W., Zhu, D., 2008. Adsorption of nonionic aromatic compounds to single-walled carbon nanotubes: effects of aqueous solution chemistry. Environ. Sci. Technol. 42 (19), 7225–7230.
Chen, J., Wang, X., Huang, Y., Lv, S., Cao, X., Yun, J., Cao, D., 2019. Adsorption removal of pollutant dyes in wastewater by nitrogen-doped porous carbons derived from natural leaves. Eng. Sci. 5, 30–38.
Chen, V., Fane, A.G., Madaeni, S., Wenten, I.G., 1997. Particle deposition during membrane filtration of colloids: transition between concentration polarization and cake formation. J. Membr. Sci. 125 (1), 109–122.
Chowdhury, S., Balasubramanian, R., 2014. Recent advances in the use of graphene-family nanoadsorbents for removal of toxic pollutants from wastewater. Adv. Colloid Interface Sci. 204, 35–56.
Chu, H.P., Li, X.Y., 2005. Membrane fouling in a membrane bioreactor (MBR): sludge cake formation and fouling characteristics. Biotechnol. Bioeng. 90 (3), 323–331.
Chu, K.H., Huang, Y., Yu, M., Her, N., Flora, J.R.V., Park, C.M., Kim, S., Cho, J., Yoon, Y., 2016. Evaluation of humic acid and tannic acid fouling in graphene oxide-coated ultrafiltration membranes. ACS Appl. Mater. Interfaces 8 (34), 22270–22279.
Chu, K.H., Shankar, V., Park, C.M., Sohn, J., Jang, A., Yoon, Y., 2017. Evaluation of fouling mechanisms for humic acid molecules in an activated biochar-ultrafiltration hybrid system. Chem. Eng. J. 326, 240–248.
Corbel, S., Mougin, C., Bouaicha, N., 2014. Cyanobacterial toxins: modes of actions, fate in aquatic and soil ecosystems, phytotoxicity and bioaccumulation in agricultural crops. Chemosphere 96, 1–15.
Cunha, G.D., Pinho, N.C., Silva, I.A.A., Costa, J.A.S., da Silva, C.M.P., Romao, L.P.C., 2019. Removal of heavy crude oil from water surfaces using a magnetic inorganic-organic hybrid powder and membrane system. J. Environ. Manag. 247, 9–18.
Didaskalou, C., Buyuktiryaki, S., Kecili, R., Fonte, C.P., Szekely, G., 2017. Valorisation of agricultural waste with an adsorption/nanofiltration hybrid process: from materials to sustainable process design. Green Chem. 19 (13), 3116–3125.
Ejraei, A., Aroon, M.A., Saravani, A.Z., 2019. Wastewater treatment using a hybrid system combining adsorption, photocatalytic degradation and membrane filtration processes. J. Water Process Eng. 28, 45–53.
Esmaeili, A., Sadeghi, E., 2014. The efficiency of Penicillium commune for bioremoval of industrial oil. Int. J. Environ. Sci. Technol. 11 (5), 1271–1276.
Esmaeili, A., Saremnia, B., 2018. Comparison study of adsorption and nanofiltration methods for removal of total petroleum hydrocarbons from oil-field wastewater. J. Petrol. Sci. Eng. 171, 403–413.
Fabris, R., Lee, E.K., Chow, C.W.K., Chen, V., Drikas, M., 2007. Pre-treatments to reduce fouling of low pressure micro-filtration (MF) membranes. J. Membr. Sci. 289 (1–2), 231–240.
Forgacs, E., Cserhati, T., Oros, G., 2004. Removal of synthetic dyes from wastewaters: a review. Environ. Int. 30 (7), 953–971.
Gao, C., Deng, W., Pan, F., Feng, X., Li, Y., 2020. Graphene and graphene oxide-based membranes for gas separation. Eng. Sci. 9, 35–43.

Gong, H., Jin, Z.Y., Wang, Q.B., Zuo, J.N., Wu, J., Wang, K.J., 2017. Effects of adsorbent cake layer on membrane fouling during hybrid coagulation/adsorption microfiltration for sewage organic recovery. Chem. Eng. J. 317, 751–757.
Guler, E., Kabay, N., Yuksel, M., Yigit, N.O., Kitis, M., Bryjak, M., 2011. Integrated solution for boron removal from seawater using RO process and sorption-membrane filtration hybrid method. J. Membr. Sci. 375 (1–2), 249–257.
Gulicovski, J.J., Cerovic, L.S., Milonjin, S.K., 2008. Point of zero charge and isoelectric point of alumina. Mater. Manuf. Process. 23 (6), 615–619.
Ha, T.W., Choo, K.H., Choi, S.J., 2004. Effect of chlorine on adsorption/ultrafiltration treatment for removing natural organic matter in drinking water. J. Colloid Interface Sci. 274 (2), 587–593.
Heo, J., Flora, J.R.V., Her, N., Park, Y.G., Cho, J., Son, A., Yoon, Y., 2012a. Removal of bisphenol A and 17 beta-estradiol in single walled carbon nanotubes-ultrafiltration (SWNTs-UF) membrane systems. Separ. Purif. Technol. 90, 39–52.
Heo, J., Joseph, L., Yoon, Y., Park, Y.G., Her, N., Sohn, J., Yoon, S.H., 2011. Removal of micropollutants and NOM in carbon nanotube-UF membrane system from seawater. Water Sci. Technol. 63 (11), 2737–2744.
Heo, J., Kim, H., Her, N., Lee, S., Park, Y.G., Yoon, Y., 2012b. Natural organic matter removal in single-walled carbon nanotubes-ultrafiltration membrane systems. Desalination 298, 75–84.
Hilbrandt, I., Shemer, H., Ruhl, A.S., Semiat, R., Jekel, M., 2019. Comparing fine particulate iron hydroxide adsorbents for the removal of phosphate in a hybrid adsorption/ultrafiltration system. Separ. Purif. Technol. 221, 23–28.
Hong, J., Kang, L., Shi, X., Wei, R., Mai, X., Pan, D., Naik, N., Guo, Z., 2022. Highly efficient removal of trace lead (II) from wastewater by 1,4-dicarboxybenzene modified Fe/Co metal organic nanosheets. J. Mater. Sci. Technol. 98, 212–218.
Huang, Z., Ong, S.L., Ng, H.Y., 2011. Submerged anaerobic membrane bioreactor for low-strength wastewater treatment: effect of HRT and SRT on treatment performance and membrane fouling. Water Res. 45 (2), 705–713.
Huber, S.A., 1998. Evidence for membrane fouling by specific TOC constituents. Desalination 119 (1–3), 229–234.
Huerta-Fontela, M., Galceran, M.T., Ventura, F., 2011. Occurrence and removal of pharmaceuticals and hormones through drinking water treatment. Water Res. 45 (3), 1432–1442.
Im, J.K., Heo, J., Boateng, L.K., Her, N., Flora, J.R.V., Yoon, J., Zoh, K.D., Yoon, Y., 2013. Ultrasonic degradation of acetaminophen and naproxen in the presence of single-walled carbon nanotubes. J. Hazard Mater. 254, 284–292.
Ipek, I.Y., Kabay, N., Yuksel, M., Yapici, D., Yuksel, U., 2012. Application of adsorption-ultrafiltration hybrid method for removal of phenol from water by hypercrosslinked polymer adsorbents. Desalination 306, 24–28.
Ji, L., Liu, F., Xu, Z., Zheng, S., Zhu, D., 2010. Adsorption of pharmaceutical antibiotics on template-synthesized ordered micro-and mesoporous carbons. Environ. Sci. Technol. 44 (8), 3116–3122.
Jiang, M.Q., Jin, X.Y., Lu, X.Q., Chen, Z.L., 2010. Adsorption of Pb(II), Cd(II), Ni(II) and Cu(II) onto natural kaolinite clay. Desalination 252 (1–3), 33–39.
Jirankova, H., Cakl, J., Markvartova, O., Dolecek, P., 2007. Combined membrane process at wastewater treatment. Separ. Purif. Technol. 58 (2), 299–303.
Joss, A., Zabczynski, S., Gobel, A., Hoffmann, B., Loffler, D., McArdell, C.S., Ternes, T.A., Thomsen, A., Siegrist, H., 2006. Biological degradation of pharmaceuticals in municipal wastewater treatment: proposing a classification scheme. Water Res. 40 (8), 1686–1696.
Jun, B.M., Elanchezhiyan, S.S., Yoon, Y., Wang, D.J., Kim, S., Prabhu, S.M., Park, C.M., 2020. Accelerated photocatalytic degradation of organic pollutants over carbonate -rich lanthanum -substituted zinc spinel ferrite assembled reduced graphene oxide by ultraviolet (UV) -activated persulfate. Chem. Eng. J. 393, 124733.
Jun, B.M., Kim, S., Heo, J., Park, C.M., Her, N., Jang, M., Huang, Y., Han, J., Yoon, Y., 2019a. Review of MXenes as new nanomaterials for energy storage/delivery and selected environmental applications. Nano Res 12 (3), 471–487.
Jun, B.M., Kim, S., Kim, Y., Her, N., Heo, J., Han, J., Jang, M., Park, C.M., Yoon, Y., 2019b. Comprehensive evaluation on removal of lead by graphene oxide and metal organic framework. Chemosphere 231, 82–92.
Jung, C., Boateng, L.K., Flora, J.R.V., Oh, J., Braswell, M.C., Son, A., Yoon, Y., 2015. Competitive adsorption of selected non-steroidal anti-inflammatory drugs on activated biochars: experimental and molecular modeling study. Chem. Eng. J. 264, 1–9.
Jung, C., Heo, J., Han, J., Her, N., Lee, S.J., Oh, J., Ryu, J., Yoon, Y., 2013a. Hexavalent chromium removal by various adsorbents: powdered activated carbon, chitosan, and single/multi-walled carbon nanotubes. Separ. Purif. Technol. 106, 63–71.
Jung, C., Park, J., Lim, K.H., Park, S., Heo, J., Her, N., Oh, J., Yun, S., Yoon, Y., 2013b. Adsorption of selected endocrine disrupting compounds and pharmaceuticals on activated biochars. J. Hazard Mater. 263 Pt 2, 702–710.
Kabay, N., Koseoglu, P., Yavuz, E., Yuksel, U., Yuksel, M., 2013. An innovative integrated system for boron removal from geothermal water using RO process and ion exchange-ultrafiltration hybrid method. Desalination 316, 1–7.
Kalaruban, M., Loganathan, P., Kandasamy, J., Vigneswaran, S., 2018. Submerged membrane adsorption hybrid system using four adsorbents to remove nitrate from water. Environ. Sci. Pollut. Res. 25 (21), 20328–20335.
Kang, S.K., Choo, K.H., 2010. Why does a mineral oxide adsorbent control fouling better than powdered activated carbon in hybrid ultrafiltration water treatment? J. Membr. Sci. 355 (1–2), 69–77.
Katsumata, H., Kaneco, S., Inomata, K., Itoh, K., Funasaka, K., Masuyama, K., Suzuki, T., Ohta, K., 2003. Removal of heavy metals in rinsing wastewater from plating factory by adsorption with economical viable materials. J. Environ. Manag. 69 (2), 187–191.
Khan, M.M.T., Takizawa, S., Lewandowski, Z., Jones, W.L., Camper, A.K., Katayama, H., Kurisu, F., Ohgaki, S., 2011. Membrane fouling due to dynamic particle size changes in the aerated hybrid PAC-MF system. J. Membr. Sci. 371 (1–2), 99–107.
Khan, M.M.T., Takizawa, S., Lewandowski, Z., Rahman, M.H., Komatsu, K., Nelson, S.E., Kurisu, F., Camper, A.K., Katayama, H., Ohgaki, S., 2013. Combined effects of EPS and HRT enhanced biofouling on a submerged and hybrid PAC-MF membrane bioreactor. Water Res. 47 (2), 747–757.
Kim, J., Cai, Z.X., Benjamin, M.M., 2010. NOM fouling mechanisms in a hybrid adsorption/membrane system. J. Membr. Sci. 349 (1–2), 35–43.
Kim, J.H., Kim, S., Lee, C.H., Kwon, H.H., Lee, S., 2008. A novel nanofiltration hybrid system to control organic micro-pollutants: application of dual functional adsorbent/catalyst. Desalination 231 (1–3), 276–282.
Kim, K.Y., Kim, H.S., Kim, J., Nam, J.W., Kim, J.M., Son, S., 2009. A hybrid microfiltration-granular activated carbon system for water purification and wastewater reclamation/reuse. Desalination 243 (1–3), 132–144.
Kim, S., Chu, K.H., Al-Hamadani, Y.A.J., Park, C.M., Jang, M., Kim, D.H., Yu, M., Heo, J., Yoon, Y., 2018. Removal of contaminants of emerging concern by membranes in water and wastewater: a review. Chem. Eng. J. 335, 896–914.
Kim, S., Munoz-Senmache, J.C., Jun, B.M., Park, C.M., Jang, A., Yu, M., Hernandez-Maldonado, A.J., Yoon, Y., 2020a. A metal organic framework-ultrafiltration hybrid system for removing selected pharmaceuticals and natural organic matter. Chem. Eng. J. 382, 122920.
Kim, S., Park, C.M., Jang, A., Jang, M., Hernandez-Maldonado, A.J., Yu, M., Heo, J., Yoon, Y., 2019. Removal of selected pharmaceuticals in an ultrafiltration-activated biochar hybrid system. J. Membr. Sci. 570, 77–84.
Kim, S., Yu, M., Yoon, Y., 2020b. Fouling and retention mechanisms of selected cationic and anionic cyes in a $Ti_3C_2T_x$ MXene-Ultrafiltration Hybrid System. ACS Appl. Mater. Interfaces 12 (14), 16557–16565.
Kong, Y., Shi, D.Q., Yu, H.W., Wang, Y.F., Yang, J.R., Zhang, Y.Y., 2006. Separation performance of polyimide nanofiltration membranes for solvent recovery from dewaxed lube oil filtrates. Desalination 191 (1–3), 254–261.
Lee, J.W., Choi, S.P., Thiruvenkatachari, R., Shim, W.G., Moon, H., 2006a. Submerged microfiltration membrane coupled with alum coagulation/powdered activated carbon adsorption for complete decolorization of reactive dyes. Water Res. 40 (3), 435–444.
Lee, J.W., Chun, J.I., Jung, H.J., Kwak, D.H., Ramesh, T., Shim, W.G., Moon, H., 2005. Comparative studies on coagulation and adsorption as a pretreatment method for the performance improvement of submerged MF membrane for secondary domestic wastewater treatment. Separ. Sci. Technol. 40 (13), 2613–2632.
Lee, N., Amy, G., Croue, J.P., 2006b. Low-pressure membrane (MF/UF) fouling associated with allochthonous versus autochthonous natural organic matter. Water Res. 40 (12), 2357–2368.
Lehmann, J., 2007. Bio-energy in the black. Front. Ecol. Environ. 5 (7), 381–387.
Li, K., Liang, H., Qu, F.S., Shao, S.L., Yu, H.R., Han, Z.S., Du, X., Li, G.B., 2014. Control of natural organic matter fouling of ultrafiltration membrane by adsorption pretreatment: comparison of mesoporous adsorbent resin and powdered activated carbon. J. Membr. Sci. 471, 94–102.
Li, M.H., Yang, Y., 2016. A cross-cultural study on a resilience-stress path model for college students. J. Counds. Dev. 94 (3), 319–332.
Lin, C., Qiao, Z., Zhang, J., Tang, J., Zhang, Z., Guo, Z., 2019. Highly efficient fluoride adsorption in domestic water with RGO/Ag nanomaterials. Eng. Sci. 4, 27–33.
Liu, H., Mao, Y., 2021. Graphene oxide-based nanomaterials for uranium adsorptive uptake. ES Mater. Manuf. 13, 3–22.
Ma, J., Yu, F., Zhou, L., Jin, L., Yang, M.X., Luan, J.S., Tang, Y.H., Fan, H.B., Yuan, Z.W., Chen, J.H., 2012. Enhanced adsorptive removal of methyl orange and methylene blue from aqueous solution by alkali-activated multiwalled carbon nanotubes. ACS Appl. Mater. Interfaces 4 (11), 5749–5760.
Ma, L.Q., Falkowski, J.M., Abney, C., Lin, W.B., 2010. A series of isoreticular chiral metal-organic frameworks as a tunable platform for asymmetric catalysis. Nat. Chem. 2 (10), 838–846.
Machado, L.E., Kist, L.T., Schmidt, R., Hoeltz, J.M., Dalberto, D., Alcayaga, E.L.A., 2007. Secondary hospital wastewater detoxification and disinfection by advanced oxidation processes. Environ. Technol. 28 (10), 1135–1143.
Maimoun, B., Djafer, A., Djafer, L., Marin-Ayral, R.M., Ayral, A., 2020. Wastewater treatment using a hybrid process coupling adsorption on marl and microfiltration. Membr. Water Treat. 11 (4), 275–282.
Matin, A., Baig, U., Gondal, M.A., Akhtar, S., Zubair, S.M., 2018. Facile fabrication of superhydrophobic/superoleophilic microporous membranes by spray-coating ytterbium oxide particles for efficient oil-water separation. J. Membr. Sci. 548, 390–397.
Mauter, M.S., Elimelech, M., 2008. Environmental applications of carbon-based nanomaterials. Environ. Sci. Technol. 42 (16), 5843–5859.
Meier, J., Melin, T., 2005. Wastewater reclamation by the PAC-NF process. Desalination 178 (1–3), 27–40.
Mozia, S., Tomaszewska, M., 2004. Treatment of surface water using hybrid processes adsorption on PAC and ultrafiltration. Desalination 162 (1–3), 23–31.
Mulyati, S., Syawaliah, S., 2018. Removal of Cd^{2+} and $^{Pb2+}$ heavy metals in water by using adsorption-ultrafiltration hybrid process. Jurnal Teknologi 80 (3–2), 17–22.
Nedzarek, A., Drost, A., Harasimiuk, F.B., Torz, A., 2015. The influence of pH and BSA on the retention of selected heavy metals in the nanofiltration process using ceramic membrane. Desalination 369, 62–67.
Nguyen, L.N., Hai, F.I., Kang, J.G., Price, W.E., Nghiem, L.D., 2012. Removal of trace organic contaminants by a membrane bioreactor-granular activated carbon (MBR-GAC) system. Bioresour. Technol. 113, 169–173.
Nguyen, T.H., Cho, H.-H., Poster, D.L., Ball, W.P., 2007. Evidence for a pore-filling mechanism in the adsorption of aromatic hydrocarbons to a natural wood char. Environ. Sci. Technol. 41 (4), 1212–1217.
Nidamanuri, N., Li, Y., Dong, M., 2020. Graphene and graphene oxide-based membranes for gas separation. Eng. Sci. 9, 3–16.

Nigra, A.E., Navas-Acien, A., 2020. Arsenic in US correctional facility drinking water, 2006-2011. Environ. Res. 188, 109768.
Nur, T., Loganathan, P., Johir, M.A.H., Kandasamy, J., Vigneswaran, S., 2018. Removing rubidium using potassium cobalt hexacyanoferrate in the membrane adsorption hybrid system. Separ. Purif. Technol. 191, 286–294.
Onderkova, B., Schlosser, S., Blahusiak, M., Bugel, M., 2009. Microfiltration of suspensions of microparticulate boron adsorbent through a ceramic membrane. Desalination 241 (1–3), 148–155.
Osawa, H., Lohwacharin, J., Takizawa, S., 2017. Controlling disinfection by-products and organic fouling by integrated ferrihydrite-microfiltration process for surface water treatment. Separ. Purif. Technol. 176, 184–192.
Pan, B., Xing, B.S., 2008. Adsorption mechanisms of organic chemicals on carbon nanotubes. Environ. Sci. Technol. 42 (24), 9005–9013.
Papic, S., Koprivanac, N., Bozic, A.L., Metes, A., 2004. Removal of some reactive dyes from synthetic wastewater by combined Al(III) coagulation/carbon adsorption process. Dyes Pigments 62 (3), 291–298.
Pearce, G., 2007. Introduction to membranes: membrane selection. Filtrat. Separ. 44 (3), 35–37.
Perreault, F., Tousley, M.E., Elimelech, M., 2014. Thin-film composite polyamide membranes functionalized with biocidal graphene oxide nanosheets. Environ. Sci. Technol. Lett. 1 (1), 71–76.
Peydayesh, M., Mohammadi, T., Bakhtiari, O., 2018. Effective treatment of dye wastewater via positively charged TETA-MWCNT/PES hybrid nanofiltration membranes. Separ. Purif. Technol. 194, 488–502.
Rafatullah, M., Sulaiman, O., Hashim, R., Ahmad, A., 2010. Adsorption of methylene blue on low-cost adsorbents: a review. J. Hazard Mater. 177 (1), 70–80.
Rerkasem, B., Jamjod, S., Pusadee, T., 2020. Productivity limiting impacts of boron deficiency, a review. Plant Soil 455 (1–2), 23–40.
Rodenas, T., Luz, I., Prieto, G., Seoane, B., Miro, H., Corma, A., Kapteijn, F., Xamena, F., Gascon, J., 2015. Metal-organic framework nanosheets in polymer composite materials for gas separation. Nat. Mater. 14 (1), 48–55.
Ryu, J., Oh, J., Snyder, S.A., Yoon, Y., 2014. Determination of micropollutants in combined sewer overflows and their removal in a wastewater treatment plant (Seoul, South Korea). Environ. Monit. Assess. 186 (5), 3239–3251.
Sablani, S.S., Goosen, M.F.A., Al-Belushi, R., Wilf, M., 2001. Concentration polarization in ultrafiltration and reverse osmosis: a critical review. Desalination 141 (3), 269–289.
Sang, G.L., Xu, P., Yan, T., Murugadoss, V., Naik, N., Ding, Y.S., Guo, Z.H., 2021. Interface engineered microcellular magnetic conductive polyurethane nanocomposite foams for electromagnetic interference shielding. Nano-Micro Lett. 13, 153.
Samatya, S., Koseoglu, P., Kabay, N., Tuncel, A., Yuksel, M., 2015. Utilization of geothermal water as irrigation water after boron removal by monodisperse nanoporous polymers containing NMDG in sorption-ultrafiltration hybrid process. Desalination 364, 62–67.
Sarasa, J., Roche, M.P., Ormad, M.P., Gimeno, E., Puig, A., Ovelleiro, J.L., 1998. Treatment of a wastewater resulting from dyes manufacturing with ozone and chemical coagulation. Water Res. 32 (9), 2721–2727.
Sarasidis, V.C., Plakas, K.V., Karabelas, A.J., 2017. Novel water-purification hybrid processes involving in-situ regenerated activated carbon, membrane separation and advanced oxidation. Chem. Eng. J. 328, 1153–1163.
Saththasivam, J., Wang, K., Yiming, W., Liu, Z., Mahmoud, K.A., 2019. A flexible $Ti_3C_2T_x$ (MXene)/paper membrane for efficient oil/water separation. RCS Adv 9, 16296.
Schlusener, M.P., Bester, K., 2006. Persistence of antibiotics such as macrolides, tiamulin and salinomycin in soil. Environ. Pollut. 143 (3), 565–571.
Secondes, M.F.N., Naddeo, V., Belgiorno, V., Ballesteros, F., 2014. Removal of emerging contaminants by simultaneous application of membrane ultrafiltration, activated carbon adsorption, and ultrasound irradiation. J. Hazard Mater. 264, 342–349.
Senguttuvan, S., Senthilkumar, P., Janaki, V., Kamala-Kannan, S., 2021. Significance of conducting polyaniline based composites for the removal of dyes and heavy metals from aqueous solution and wastewaters - a review. Chemosphere 267, 129201.
Serrano, D., Suarez, S., Lema, J.M., Omil, F., 2011. Removal of persistent pharmaceutical micropollutants from sewage by addition of PAC in a sequential membrane bioreactor. Water Res. 45 (16), 5323–5333.
Shao, S.L., Liang, H., Qu, F.S., Li, K., Chang, H.Q., Yu, H.R., Li, G.B., 2016. Combined influence by humic acid (HA) and powdered activated carbon (PAC) particles on ultrafiltration membrane fouling. J. Membr. Sci. 500, 99–105.
Shemer, H., Melki-Dabush, N., Semiat, R., 2019. Removal of silica from brackish water by integrated adsorption/ultrafiltration process. Environ. Sci. Pollut. Res. 26 (31), 31623–31631.
Shi, X.F., Field, R., Hankins, N., 2011. Review of fouling by mixed feeds in membrane filtration applied to water purification. Desalin. Water Treat. 35 (1–3), 68–81.
Shi, X., Hong, J., Wang, C., Kong, S., Li, J., Pan, D., Lin, J., Jiang, Q., Guo, Z., 2021. Preparation of Mg,N-co-doped lignin adsorbents for enhanced selectivity and high adsorption capacity of as (V) from wastewater. Particuology 58, 206–213.
Shoushtarian, F., Negahban-Azar, M., 2020. Worldwide regulations and guidelines foragricultural water reuse: a critical review. Water 12 (4), 971.
Snyder, S.A., Westerhoff, P., Yoon, Y., Sedlak, D.L., 2003. Pharmaceuticals, personal care products, and endocrine disruptors in water: implications for the water industry. Environ. Eng. Sci. 20 (5), 449–469.
Srihari, V., Das, A., 2008. Comparative studies on adsorptive removal of phenol by three agro-based carbons: equilibrium and isotherm studies. Ecotoxicol. Environ. Saf. 71 (1), 274–283.
Talbot, D., Bee, A., Treiner, C., 2003. Adsolubilization of 4-nitrophenol at a kaolinite/water interface as a function of pH and surfactant surface coverage. J. Colloid Interface Sci. 258 (1), 20–26.
Tang, Y., Tang, B.B., Wu, P.Y., 2015. Preparation of a positively charged nanofiltration membrane based on hydrophilic-hydrophobic transformation of a poly(ionic liquid). J. Mater. Chem. 3 (23), 12367–12376.
Tanis, E., Hanna, K., Emmanuel, E., 2008. Experimental and modeling studies of sorption of tetracycline onto iron oxides-coated quartz. Colloids Surf., A 327 (1–3), 57–63.
Thunemann, A.F., Schutt, D., Kaufner, L., Pison, U., Mohwald, H., 2006. Maghemite nanoparticles protectively coated with poly(ethylene imine) and poly(ethylene oxide)-block-poly(glutamic acid). Langmuir 22 (5), 2351–2357.
Tomaszewska, M., Mozia, S., 2002. Removal of organic matter from water by PAC/UF system. Water Res. 36 (16), 4137–4143.
Torabian, A., Kazemian, H., Seifi, L., Bidhendi, G.N., Azimi, A.A., Ghadiri, S.K., 2010. Removal of petroleum aromatic hydrocarbons by surfactant-modified natural zeolite: the effect of surfactant. Clean 38 (1), 77–83.
Ullah, A., Zahoor, M., Alam, S., Ullah, R., Alqahtani, A.S., Mahmood, H.M., 2019. Separation of levofloxacin from industry effluents using novel magnetic nanocomposite and membranes hybrid processes. BioMed Res. Int. 2019, 5276841.
Usman, M., Katsoyiannis, I., Rodrigues, J.H., Ernst, M., 2021. Arsenate removal from drinking water using by-products from conventional iron oxyhydroxides production as adsorbents coupled with submerged microfiltration unit. Environ. Sci. Pollut. Res. 1238.
Wang, H., Qu, F.S., Ding, A., Liang, H., Jia, R.B., Li, K., Bai, L.M., Chang, H.Q., Li, G.B., 2016. Combined effects of PAC adsorption and in situ chlorination on membrane fouling in a pilot-scale coagulation and ultrafiltration process. Chem. Eng. J. 283, 1374–1383.
Wang, X.M., Phillips, B.L., Boily, J.F., Hu, Y.F., Hu, Z., Yang, P., Feng, X.H., Xu, W.Q., Zhu, M.Q., 2019. Phosphate sorption speciation and precipitation mechanisms on amorphous aluminum hydroxide. Soil Syst 3 (1), 20.
Westerhoff, P., Yoon, Y., Snyder, S., Wert, E., 2005. Fate of endocrine-disruptor, pharmaceutical, and personal care product chemicals during simulated drinking water treatment processes. Environ. Sci. Technol. 39 (17), 6649–6663.
Xie, P.T., Liu, Y., Feng, M., Niu, M., Liu, C.Z., Wu, N.N., Sui, K.Y., Patil, R.R., Pan, D., Guo, Z.H., Fan, R.H., 2021. Hierarchically porous Co/C nanocomposites for ultralight high-performance microwave absorption. Adv. Compos. Hyb. Mater. 4, 173–185.
Xu, Y., Gu, P., Zhang, G.H., Wang, X.Q., 2017. Investigation of coagulation as a pretreatment for microfiltration in cesium removal by copper ferrocyanide adsorption. J. Radioanal. Nucl. Chem. 313 (2), 435–444.
Yoo, D.K., Yoon, T.U., Bae, Y.S., Jhung, S.H., 2020. Metal-organic framework MIL-101 loaded with polymethacrylamide with or without further reduction: effective and selective CO_2 adsorption with amino or amide functionality. Chem. Eng. J. 380, 122496.
Yoon, J., Amy, G., Chung, J., Sohn, J., Yoon, Y., 2009. Removal of toxic ions (chromate, arsenate, and perchlorate) using reverse osmosis, nanofiltration, and ultrafiltration membranes. Chemosphere 77 (2), 228–235.
Yoon, Y., Amy, G., Cho, J.W., Her, N., Pellegrino, J., 2002. Transport of perchlorate (ClO_4^-) through NF and UF membranes. Desalination 147 (1–3), 11–17.
Yoon, Y., Lueptow, R.M., 2005. Removal of organic contaminants by RO and NF membranes. J. Membr. Sci. 261 (1–2), 76–86.
Yoon, Y., Ryu, J., Oh, J., Choi, B.G., Snyder, S.A., 2010. Occurrence of endocrine disrupting compounds, pharmaceuticals, and personal care products in the Han River (Seoul, South Korea). Sci. Total Environ. 408 (3), 636–643.
Yoon, Y.M., Amy, G., Cho, J.W., Her, N., 2005. Effects of retained natural organic matter (NOM) on NOM rejection and membrane flux decline with nanofiltration and ultrafiltration. Desalination 173 (3), 209–221.
Yuan, B., Li, L., Muragadoss, V., Vupputuri, S., Wang, J., Alikhani, N., Guo, Z., 2020. Nanocellulose-based composite materials for wastewater treatment and waste-oil remediation. ES Food Agro 1, 41–52.
Zahoor, M., Mahramanlioglu, M., 2011. Removal of phenolic substances from water by adsorption and adsorption-ultrafiltration. Separ. Sci. Technol. 46 (9), 1482–1494.
Zelmanov, G., Semiat, R., 2015. The influence of competitive inorganic ions on phosphate removal from water by adsorption on iron (Fe^{+3}) oxide/hydroxide nanoparticles-based agglomerates. J. Water Process Eng. 5, 143–152.
Zhang, S., Yang, Y., Takizawa, S., Hou, L.A., 2018. Removal of dissolved organic matter and control of membrane fouling by a hybrid ferrihydrite-ultrafiltration membrane system. Sci. Total Environ. 631–632, 560–569.
Zhang, S.J., Shao, T., Bekaroglu, S.S.K., Karanfil, T., 2010. Adsorption of synthetic organic chemicals by carbon nanotubes: effects of background solution chemistry. Water Res. 44 (6), 2067–2074.
Zhao, F.Y., Ji, Y.L., Weng, X.D., Mi, Y.F., Ye, C.C., An, Q.F., Gao, C.J., 2016. High-flux positively charged nanocomposite nanofiltration membranes filled with poly (dopamine) modified multiwall carbon nanotubes. ACS Appl. Mater. Interfaces 8 (10), 6693–6700.
Zheng, W., Zhang, P.G., Tian, W.B., Qin, X., Zhang, Y.M., Sun, Z.M., 2018. Alkali treated Ti3C2Tx MXenes and their dye adsorption performance. Mater. Chem. Phys. 206, 270–276.
Zhong, P.S., Widjojo, N., Chung, T.S., Weber, M., Maletzko, C., 2012. Positively charged nanofiltration (NF) membranes via UV grafting on sulfonated polyphenylenesulfone (sPPSU) for effective removal of textile dyes from wastewater. J. Membr. Sci. 417, 52–60.